

# Gas Dynamic and Thermal Perturbation of Flame by Sampling Probe

A.G. Tereshchenko, P.A. Skovorodko\*, O.P. Korobeinichev, D.A. Knyazkov, A.G. Shmakov

Institute of Chemical Kinetics & Combustion SB RAS, Novosibirsk, Russia

\* Institute of Thermophysics SB RAS, Novosibirsk, Russia

*An external flow of burner-stabilized methane-oxygen-argon flame at atmospheric pressure near an axisymmetric sampling probe representing the cone with tip and orifice in its center with accounting for the real properties of the gas is investigated. The simulation of the flow between the burner and the probe is performed in the frames of full set of unsteady Navier-Stokes equations solved numerically by recently developed original algorithm. For approximate accounting for heat release due to the chemical reactions a source term is introduced in the energy equation providing the given temperature distribution in undisturbed isobaric flame i. e. in the absence of the probe in the flame. The distribution of temperature over the probe surface is set on the basis of thermocoupled measurements. On the probe orifice surface a suction of the gas with local sonic speed is assumed for simplicity. The comparison between the steady flow near the probe (a streamlines picture, an isotherms field, etc.) and the undisturbed flame gives the qualitative representation of the character and the quantity of distortion factors induced by the probe in the flame. The calculated values of gas temperature on the flow centerline near the probe orifice are in satisfactory agreement with the measured data.*

*To simulate the probe-induced distortion of mixture composition in the flame wave the distribution of concentrations of some components ( $\text{CH}_4$ ,  $\text{CO}_2$ ,  $\text{H}_2\text{O}$  and  $\text{O}_2$ ) in the flow field is calculated in the frames of diffusion equation for binary gas mixture ( $\text{CH}_4 - \text{Ar}$ ,  $\text{CO}_2 - \text{Ar}$ , etc.) solved in a linear statement. For approximate accounting for the effect of chemical reactions the source term is introduced in the diffusion equation providing the given distribution of concentration in undisturbed flame. The calculated concentrations in the center of the probe orifice were found to be shifted downstream in comparison with undisturbed values, that is in agreement with experimental data, though the measured values of shift are noticeably higher than the calculated ones.*

*The developed approach based on the spatially fixed sources of energy and species concentrations allows one to study the probe-induced distortions of the flame flow field in the conditions closer to the real ones in comparison with the previously developed approaches available in literature.*

## INTRODUCTION

Mass-spectrometry sampling is one of the most important methods for flame diagnostics. Two types of apparatus are used to study flame structure. The sample is transported to an ion source - 1) as a molecular flow using a microprobe – a cone with an opening angle of 5 – 20 degrees, an inlet orifice of 5 – 20  $\mu\text{m}$ , and -2) as a molecular beam using a “sonic probe” with the opening angle of cone equal to or more than 40 degrees, an inlet orifice of 20 – 300  $\mu\text{m}$  and a skimmer. The microprobe has high spatial resolution and only slightly disturbs the flame, allowing the study of flames with a narrow combustion zone of 0.1 mm or less. Radicals, however, may recombine, and unstable species, including vapors of energetic materials, may decompose and react on the inner hot walls of the probe and deposit on the cold parts of the probe walls. Molecular-beam mass-spectrometric (MBMS) sampling using the “sonic probe” allows the detection of radicals and other unstable species but disturbs the flame more strongly and, therefore, has a reduced spatial resolution.

To interpret the sampling measurements correctly, the analysis of the probe-induced perturbations is needed. The distortions caused by the probe can be divided into internal and external ones, the latter being gas dynamic and thermal. The probe acts as a sink for matter and

heat, which causes distortions of temperature and species concentration profiles. As a consequence, this results in distortion of lines of equal temperature and concentration in the flame flow field, being plane one-dimensional in the absence of the probe.

The probe sampling factor  $\alpha$  seems to be one of the important parameters characterizing gas dynamic interaction between the probe and the flame. It is defined as

$$\alpha = 4Q / \pi d^2 \rho_0 w_0, \quad (1)$$

where  $Q$  is the gas flow rate through the probe orifice with diameter  $d$ ,  $\rho_0$  and  $w_0$  are the density and the velocity of undisturbed flow.

In practice, the sampling is performed not from a local point, but from a certain volume in the flame. Spatial location of this volume depends on several factors, such as sampling factor and the distance between the tip of the probe and the burning surface. The thermal interaction between the flame and the probe surface affects the chemical processes in flame as well as the sample composition. Thus, it is reasonable to take them into account while interpreting the results obtained by the sampling probe. There are many simplified theoretical approaches in literature [1-7] to resolve this problem. But till now there is no accurate solution to the problem because of its complexity.

As a result of the analysis of the problem of flame perturbation by probe it is possible to allocate two important aspects:

1. The changes in the flame structure due to the thermal and gas dynamic interaction between the probe and the flame.
2. The increase in the flow velocity along the probe centerline due to the sample suction by the probe that results in downstream shift of the isotherms and the lines of equal concentration.

The velocity field and the streamlines near the probe orifice have been first calculated by Rosen [1] for the disk sink model. However, it wasn't taken into account that a real probe represents a certain obstacle for the gas flow because of finite size of the probe.

Using the results obtained by Rosen, Ksandopulo and co-workers [2] have calculated "kinematic shift" for various  $\alpha$ . "Kinematic shift"  $\delta$  was determined as  $\delta = w_0(t - t_1)$ , where  $w_0$  is unperturbed flow velocity,  $t = z_p / w_0$  is the time required for unperturbed flow to pass the distance  $z_p$  to the probe orifice,  $t_1$  - is the time required for perturbed flow to pass the same distance. The value of  $t_1$  was calculated using the flow velocity profile.

Yi and Knuth [3] have solved a gas dynamic problem on finding out the distribution of flow parameters near the sink orifice of a conical probe. Inviscid flow was assumed and the known solution of the problem of point sink in incompressible fluid corrected for accounting for compressibility effects was used when solving this problem. The concentration evolution was treated as self-diffusion process in binary gas mixture. Comparing concentration profiles obtained with and without the probe the authors have established that these profiles may be characterized by a "shift"  $\delta$ , which is determined by a relation

$$\delta / d = 0.19(\text{Re} Sc)^{1/2}, \quad (2)$$

where  $\text{Re}$  is the Reynolds number defined by the gas parameters in the probe orifice plane and the orifice diameter,  $Sc$  is the Schmidt number.

Various aspects of the sampling probe effects in the flames were considered by Smith [4] and by Hayhurst et al. in the series of papers [5-7].

Besides theoretical considerations there are many experimental paper devoted to the problem of probe-induced perturbation of the flame.

The influence of external diameter of the "sonic" probe tip (0.5 - 2 mm) and the cone angle on  $\text{O}_2$  concentration profile in atmospheric methane/oxygen flame was studied experimentally by Yoon and Knuth [8].

"Sonic" probe effect on temperature field in low-pressure flame was studied by Hartlieb et al. using laser-induced-fluorescence of OH and NO [9]. In the vicinity of the nozzle tip the decrease of temperature due to the nozzle cooling effect was observed.

Korobeinichev et al. [10] have observed experimentally downstream shift of methane concentration profile due to the probe effect as compared to unperturbed profile in atmospheric premixed methane/oxygen/argon flame. Based on the results of Ref. [2] and the comparison of experimental data obtained with mass-spectrometric sampling technique and spectroscopic technique, the semi-empirical relation for estimation of the shift  $\delta = 0.37d\sqrt{\alpha}$  was proposed. This relation describes gas dynamic flame distortion by the probe and seems to be inapplicable in the case of strong thermal perturbation of the flame by the probe.

Thermal effect of the probe on the flame with respect to the cone angle of the probe was studied by Biordi et al. [11]. They measured temperature profiles in methane/oxygen/argon flames at  $\sim 0.04$  atm using Pt-Pt 10% Rh thermocouples directly in front of the probe tip at the distance of two orifice diameter. The decrease in gas temperature on the average of 200 K was observed for probe cone angles up to  $64^\circ$ . Moreover, a probe with the cone angle of  $78^\circ$  was found to disturb significantly the flame structure.

Probe effects in flame as well as heat-exchange between the probe and the flame were studied by Emelyanov et al. [12]. A probe with geometry close to real one was considered in that paper and the coefficients of heat-transfer between the probe and the flame were determined using experimental data.

There are several methods for measuring temperature profiles in flames: thermocouple, spectroscopic and two other methods in which sampling probe is used as a temperature measuring device. These methods are the pneumatic probe technique [13], which was used by Kaiser et al. [14] and Fisher et al. [15], and the time-of-flight (TOF) technique [8, 16]. The use of the first one for measuring the temperature profiles is based on application of the choked flow relation for the gas flow rate through the probe orifice.

One of the main goals of the flame structure study is to validate the mechanism of chemical reactions on the basis of comparison between experimental and modeling results. An interesting feature of the discussed flow that allows one to solve the above stated problem in spite of perturbation of a flame by a probe was noticed and used in Refs. [17 – 21]. Namely, during the modeling the structure of a flame stabilized on the flat burner, the temperature profile, entering the governing equations, was specified as being measured by thermocouple, which junction is located in front of the sampling tip by about two diameters of a probe orifice. These profiles are surely perturbed by the sampling, nevertheless a satisfactory agreement between calculated and measured with the help of MBMS system species concentration profiles was observed. Similar approach was applied in Ref. [15] where perturbed temperature profiles were obtained by choked probe technique. These results reflect the deep internal relation between local temperature and mixture composition in the flame flow perturbed by the probe, though the range of applicability of such approach is not completely clarified.

The number of papers devoted to study of the probe-induced perturbation of flame is very high and only some part of them was referenced here. It should be noted, however, that theoretical approaches applied previously to the analysis of gas dynamic effects of the probe were highly simplified. As a rule, these approaches were based on approximation of the flow field near the probe by incompressible fluid flow with particular geometry of the probe being not taken into account. Therefore, the purpose of the present paper is to develop a model for probe-induced distortions with accounting for the main features of the flame flow and the real geometry of the probe. The results of simulation are analyzed and compared with experimental data on the flame structure obtained in a flat, premixed, fuel-lean methane/oxygen/argon flame at 1 atm by mass-spectrometric sampling technique and microthermocouple technique.

## 1. EXPERIMENTAL

Premixed laminar  $\text{CH}_4/\text{O}_2/\text{Ar}$  flame was stabilized on a Botha-Spalding burner 16 mm in diameter at atmospheric pressure and slightly elevated unburned gas temperature of about 368 K. Combustible  $\text{CH}_4/\text{O}_2/\text{Ar}$  mixture (lean, 0.06/0.15/0.79) was prepared using mass flow controllers, with a total volumetric flow rate of  $25 \text{ cm}^3/\text{s}$ . An uniform distribution of flow velocity was reached

with a help of brass disc with holes 0.5 mm in diameter. The burner was moved along its axis to provide the sampling by a fixed probe.

Temperature measurements in the flame were performed by Pt-Pt+10%Rh thermocouple welded from wire 0.02 mm in diameter, covered by a thin layer of SiO<sub>2</sub> to prevent catalytic recombination of radicals on their surface. The resulting thermocouple junction has a diameter of 0.03 mm and a shoulder length of about 4 mm, providing negligible heat losses to the cold contacts. Further details of the thermocouple design can be found elsewhere [22]. The thermocouple is mounted on a holder which enables its moving in three directions.

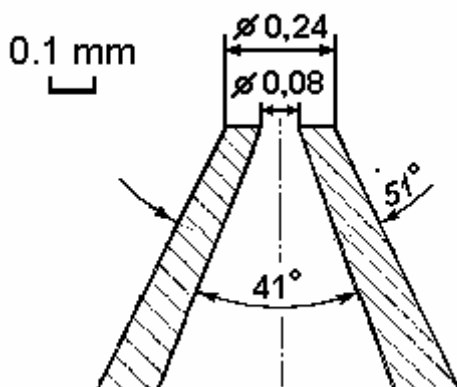


Fig. 1. The sketch of the probe.

CH<sub>4</sub> and H<sub>2</sub>O spatial profiles were measured using two techniques: molecular-beam mass-spectrometry (MBMS) technique and a technique based on molecular leakage through the probe connected to the inlet system of quadrupole mass-spectrometer MS-7302. Molecular-beam setup based on quadrupole mass-spectrometer MS-7302 was detailed previously [22, 23].

In all measurements the same quartz so-called “sonic” probe was used. The probe is sketched in Fig. 1, where all sizes are given. The probe was mounted on a water-cooled stainless steel flange which was translatable in order to fasten it either to the MBMS setup or to the molecular leakage system.

To calculate the flame flow near the probe the boundary conditions for temperature on the probe surface should be specified. The measurements of the temperature of the probe tip and the probe walls at various distances from the tip were performed by the thermocouple. The position of the thermocouple junction was controlled by a cathetometer.

## 2. NUMERICAL ALGORITHM

The simulation of the flow between the burner and the axisymmetric probe inserted in the flow is performed in the frames of the full set of unsteady Navier-Stokes equations. For approximate accounting for heat release due to the chemical reactions the source term is introduced in the energy equation providing the given temperature distribution in the plane undisturbed isobaric flame i. e. in the absence of the probe in the flame.

The main features of the recently developed original algorithm used to solve the Navier-Stokes equations are described below.

### 2.1. The governing equations

The governing system of equations for two-dimensional flow with plane ( $v = 0$ ) or axial ( $v = 1$ ,  $y$ ,  $z$  - radial and axial coordinates, respectively) types of symmetry have the usual form and includes the continuity equation

$$\frac{D\rho}{Dt} + \rho \cdot \text{div } \vec{v} = 0, \quad (3)$$

two momentum equations

$$\rho \frac{Du}{Dt} + \frac{\partial p}{\partial y} = \frac{\partial \tau_{yy}}{\partial y} + v \frac{\tau_{yy} - \tau_{\theta\theta}}{y} + \frac{\partial \tau_{yz}}{\partial z}, \quad (4)$$

$$\rho \frac{Dw}{Dt} + \frac{\partial p}{\partial z} = \frac{\partial \tau_{zy}}{\partial y} + v \frac{\tau_{zy}}{y} + \frac{\partial \tau_{zz}}{\partial z}, \quad (5)$$

and the energy equation

$$\rho \frac{De}{Dt} + p \cdot \text{div } \vec{v} = -\frac{\partial q_y}{\partial y} - v \frac{q_y}{y} - \frac{\partial q_z}{\partial z} + \Phi, \quad (6)$$

where

$$\frac{D}{Dt} = \frac{\partial}{\partial t} + u \frac{\partial}{\partial y} + w \frac{\partial}{\partial z},$$

$$\text{div } \vec{v} = \frac{\partial u}{\partial y} + v \frac{u}{y} + \frac{\partial w}{\partial z},$$

$$\Phi = \tau_{yy} \frac{\partial u}{\partial y} + v \tau_{\theta\theta} \frac{u}{y} + \tau_{zz} \frac{\partial w}{\partial z} + \frac{\tau_{zy}^2}{\mu},$$

$$\tau_{yy} = 2\mu \frac{\partial u}{\partial y} + (\mu' - \frac{2}{3}\mu) \cdot \text{div } \vec{v},$$

$$\tau_{zz} = 2\mu \frac{\partial w}{\partial z} + (\mu' - \frac{2}{3}\mu) \cdot \text{div } \vec{v},$$

$$\tau_{\theta\theta} = 2\mu v \frac{u}{y} + (\mu' - \frac{2}{3}\mu) \cdot \text{div } \vec{v},$$

$$\tau_{yz} = \tau_{zy} = \mu \cdot \left( \frac{\partial u}{\partial z} + \frac{\partial w}{\partial y} \right),$$

$$q_y = -\lambda \frac{\partial T}{\partial y}, \quad q_z = -\lambda \frac{\partial T}{\partial z}.$$

Here  $u$  and  $w$  are the radial and axial components of the total velocity,  $\rho$  is the density,  $p$  is the pressure,  $T$  is the temperature,  $e$  is the specific internal energy,  $\mu$  is the dynamic viscosity,  $\mu'$  is the bulk viscosity,  $\lambda$  is the heat conductivity. To close the system of equations (3) - (6) the following relations are used assuming the gas to be perfect

$$p = \rho \cdot R \cdot T,$$

$$e = \frac{1}{\kappa - 1} \cdot R \cdot T,$$

where  $R$  is the gas constant and  $\kappa$  is the specific heats ratio.

## 2.2. The finite-difference scheme

The main features of the finite-difference scheme we have used are the following:

- i) The finite-difference approximation of the governing equations is made on a staggered grid, where pressure, density and temperature, as well as the transport coefficients, are determined in the center of the cell, while the components of velocity are determined in the middle of the corresponding borders of the cell.
- ii) The finite-difference relations are resolved implicitly with the help of the well-known method of splitting into physical processes and spatial variables [24]. On each fractional step the standard tridiagonal matrix algorithm is applied.
- iii) The continuity equation is approximated according to the scheme providing conservation of variables on reaching the steady solution (or on explicit resolving of the relations).

- iv) The centered approximation of difference operators provides the second order of accuracy over spatial variables on the uniform grid.
- v) The algorithm is characterized by low implicit artificial viscosity that essentially widens the range of Reynolds numbers accessible for modeling.

The staggered grid was proposed in Ref. [25] and is widely used for simulation of incompressible flows. Our experience indicates, however, clear advantages of this grid for simulation of highly compressible flows too [26 – 28].

### 2.3. The domain of simulation and boundary conditions

The existing version of the algorithm operates with a uniform rectangular grid with mesh sizes  $dy$  and  $dz$  in radial and axial directions. The domain of simulation may consist of some number of straight lines parallel or perpendicular to the axis and one line with arbitrary inclination to the axis. The cells in the vicinity of this line are of triangle or trapezium form that leads to some modification of the finite-difference relations here providing the second order accuracy of the scheme.

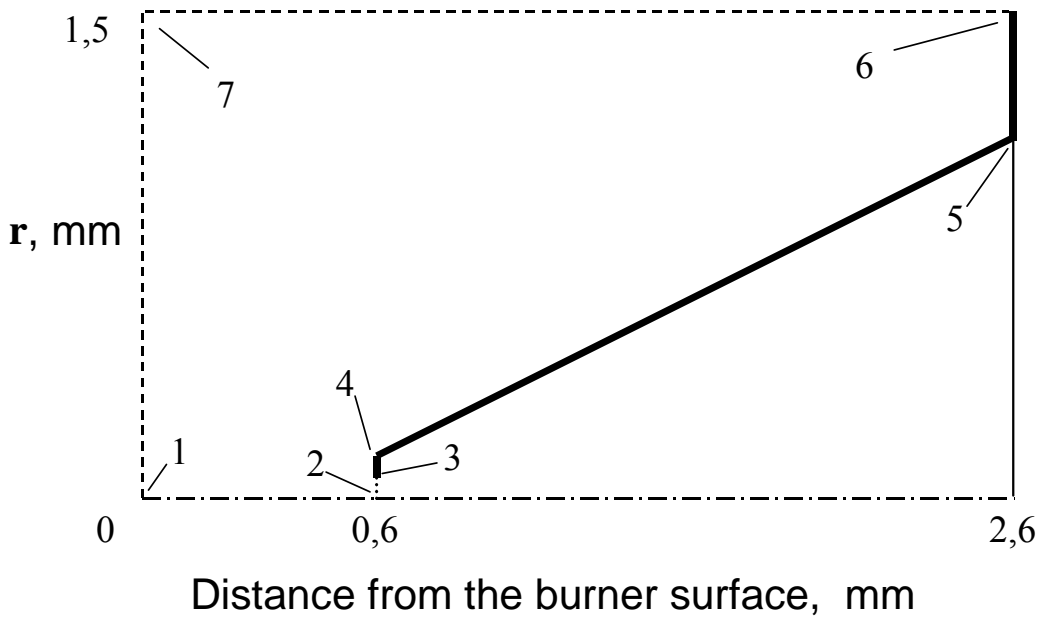


Fig. 2. Scheme of the domain of simulation.

Fig. 2 illustrates the scheme of the domain of simulation for distance between the probe and the burner  $z_0 = 0.6$  mm. The solid boundaries are shown by solid lines while the dotted lines correspond to permeable inlet and outlet boundaries. This domain correspond to the shape of the sampling probe used in our experiments (orifice diameter  $80 \mu\text{m}$ , tip diameter  $240 \mu\text{m}$  and half-angle of conical part of the probe  $25.5^\circ$ ). The burner-to-probe distance  $z_0$  was varied in the range  $0.2 - 0.8$  mm, the length of the conical part of the probe being 2 mm for all the variants.

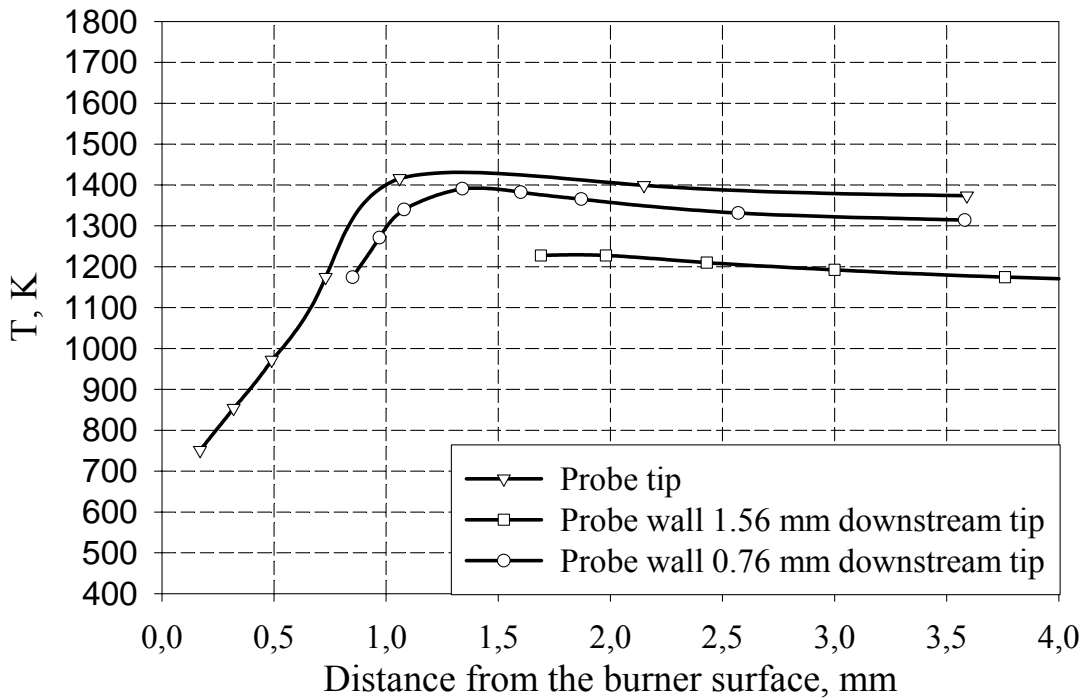
At the burner surface (line 1 – 7) the conditions for all the values were specified on the basis of the solution for isobaric undisturbed flame obtained by Chemkin code [29] for considered mixture ( $T = 368\text{K}$ ,  $w = 15.68 \text{ cm/s}$ ,  $u = 0$ ).

At the solid boundaries (lines 3-4-5-6) the normal component of total velocity ( $v_n$ ) is prescribed to be equal to zero while the tangential component ( $v_t$ ) as well as the temperature are defined taking into account the velocity slip and temperature jump [30]:

$$v_t = -\frac{2 - \alpha_v}{\alpha_v} \frac{\mu}{p} \left( \frac{\pi RT}{2} \right)^{1/2} \left( \frac{\partial v_t}{\partial n} \right)_w,$$

$$\Delta T_w = -\frac{2 - \alpha_T}{\alpha_T} \frac{2\kappa}{Pr \cdot (\kappa + 1)} \frac{\mu}{p} \left( \frac{\pi RT}{2} \right)^{1/2} \left( \frac{\partial T}{\partial n} \right)_w,$$

with two accommodation coefficients  $\alpha_v$  and  $\alpha_T$  which were assumed to be equal to 1. These conditions automatically become the no-slip conditions for velocity and the condition of the absence of a temperature jump in the flow regions where the rarefaction effects are negligibly small. The distribution of temperature over the probe surface is set on the basis of thermocoupled measurements. Figure 3 illustrates the results of these measurements for some points on the probe surface that were used for linear extrapolation of temperature along the probe cone. There is no



need to prescribe the pressure or the density at the solid boundaries.

Fig. 3. Probe wall temperatures measured by Pt/Pt10%Rh thermocouple with  $d = 20 \mu\text{m}$ .

At the probe orifice surface (line 2 - 3) all the variables except the axial velocity are specified by extrapolation from internal points of the domain while the axial velocity was prescribed to be equal to local speed of sound. This assumption allows one to exclude the consideration of internal flow inside the probe though it may lead, of course, to some inaccuracy in the flow description.

At the upper permeable boundary (line 7 - 6) an attempt was made to specify all the variables by extrapolation from interior. The simulations show, however, that for considered highly subsonic flow to obtain the stable solution it is necessary to specify the pressure on this boundary. The latter condition is equivalent to the presence of mass sources or sinks here.

At the axis of symmetry (line 1 - 2) the radial velocity as well as the radial derivatives of the axial velocity and temperature are prescribed to be zero.

The mesh size  $dy$  in radial direction was chosen to be  $2.5 \mu\text{m}$ , thus the number of grids was 16 over probe orifice radius and 48 over probe tip. The mesh size  $dz$  in axial direction slightly differs from  $dy$  and was about  $2.62 \mu\text{m}$ . The latter value is prescribed by the relation between  $dy$  and  $dz$  in the considered case with the domain containing the line with arbitrary inclination to the axis (see Fig. 2).

## 2.4. The source term for energy equation

All the simulations were performed to describe the flow of burner-stabilized premixed methane-oxygen-argon flame with initial mixture composition  $6\%CH_4 + 15\%O_2 + 79\%Ar$ .

The considered combustion-gas mixture is assumed to be a monocomponent perfect gas with molecular mass  $37.32 \text{ kg/kmole}$  and the value of the specific heats ratio  $\kappa = 1.5747$  calculated from the real parameters of the flame at the burner surface.

The temperature dependence of dynamic viscosity  $\mu$  of the gas was assumed to be described by Lennard-Jones (6 – 12) potential with parameters  $\sigma = 3.418 \text{ \AA}$ ,  $\varepsilon/k = 124 \text{ K}$  typical for argon [31]. Since the main component of considered mixture is argon, the value of Prandtl number ( $Pr = \mu C_p / \lambda$ ) was assumed to be the same as for monatomic gas, i. e.  $Pr = 2/3$ . The effect of bulk viscosity was neglected ( $\mu' = 0$ ).

For numerical solution the variables  $\rho$ ,  $p$ ,  $T$ ,  $u$  and  $w$  have been normalized by the corresponding parameters at the burner surface including the sound speed  $c_0$ . The spatial variables  $y$  and  $z$  appear to be conveniently expressed directly in mm.

As it was mentioned above, for approximate accounting for the heat release due to chemical reactions the source term  $Q_{source}(z)$  was introduced in the energy equation providing the given temperature distribution in undisturbed isobaric flame i. e. in the absence of the probe in the flame. This term depending only on  $z$  was obtained from the relation written in non-dimensional form

$$\frac{\partial T}{\partial t} = Q_{conv} + Q_{vis} + Q_{source} = 0, \quad (7)$$

where the convective terms entering the energy equation (6) are schematically denoted as  $Q_{conv}$  while the viscous terms are denoted as  $Q_{vis}$ . The finite-difference representation of the relation (7)

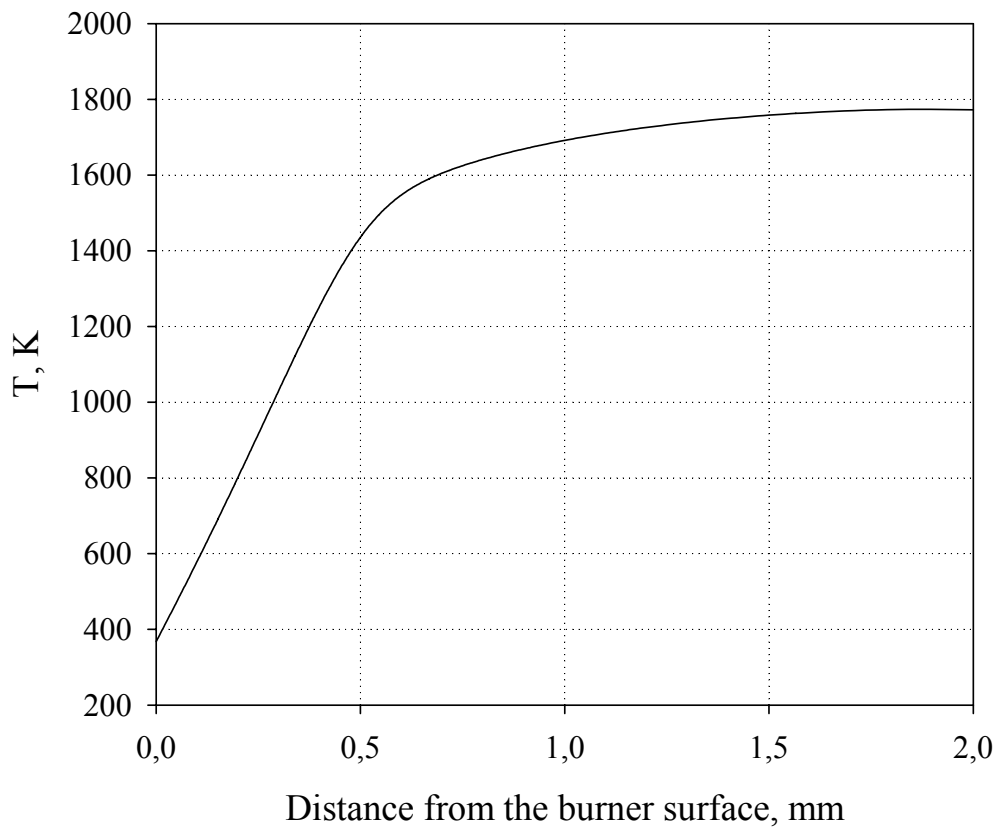


Fig. 4. Temperature distribution in undisturbed flame.

for one-dimensional flow was made on the same staggered grid for axial coordinate as in two-dimensional calculations, the values of source term being determined in the center of the cell. The temperature distribution in the flow was set in accordance with the results of simulation of undisturbed flame flow by Chemkin Premix code [29]. This distribution is shown in Fig. 4. The distribution of density and axial velocity entering the relation (7) were found from continuity equation and equation of state. To obtain the source term consistent with the considered model of the flow we neglect, therefore, small changes of the mean molecular mass that takes place in the real undisturbed flame due to the chemical reactions.

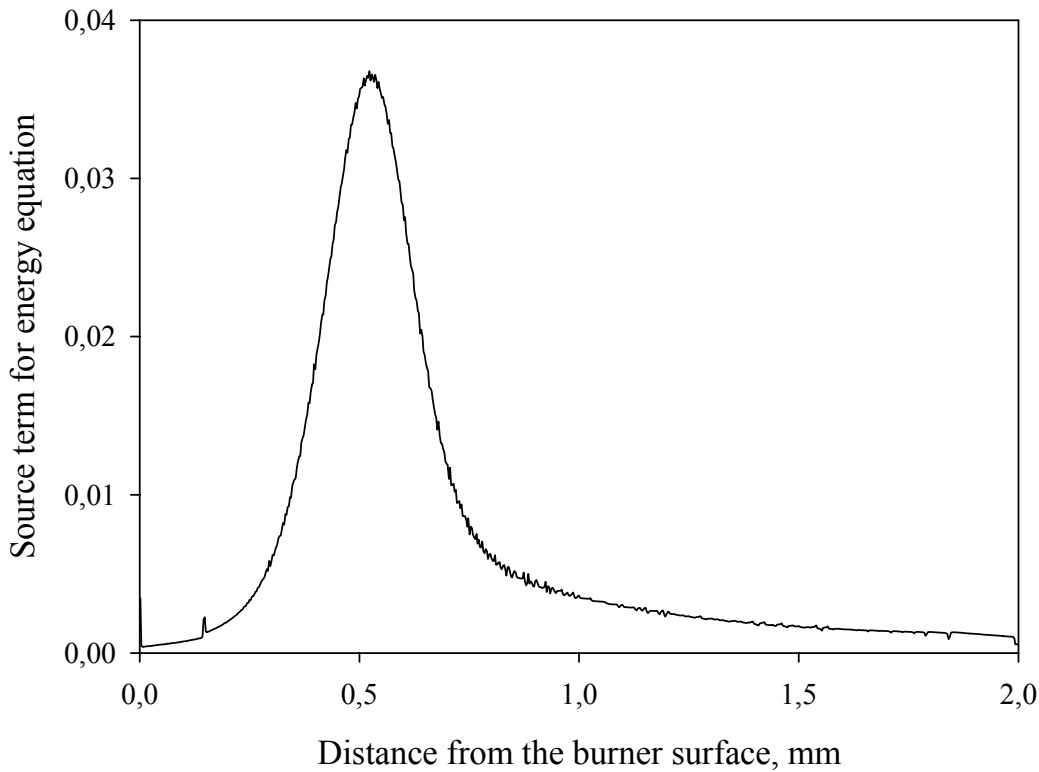


Fig. 5. The source term for energy equation.

The obtained axial dependence of  $Q_{source}(z)$  is illustrated in Fig. 5. Positive values reflect the heating effect due to the chemical reactions. The visible oscillations, which have negligibly small effect on the results, are connected with some inaccuracy during approximation of the flame parameters. In the testing two-dimensional simulation of the flow with shown source term in the case when no probe was inserted in the flow field the purely plane one-dimensional flow was obtained with good representation of the temperature distribution in undisturbed flame. We may hope, therefore, that the conditions in the flow field near the probe will be similar to those in the real flame.

## 2.5. Numerical procedure

The simulations were performed for 4 burner-to-probe distances ( $z_0$ ): 0.2, 0.4, 0.6 and 0.8 mm.

The initial distribution of the parameters in the domain of simulation was set as in undisturbed flame. The existence of the probe disturbs this distribution due to the presence of solid surfaces in the flow field, the suction of the gas by the probe orifice and the heat exchange between the gas and the probe surface. That is why the flow begins to rearrange and after some time it reaches the steady state.

We will not illustrate the numerous set of testing simulations confirming that the obtained solution of the finite-difference relations is quite adequate to the solution of initial differential equations. Some of the corresponding results were reported earlier [26–28].

### 3. GAS DYNAMIC STRUCTURE OF THE FLOW

Fig. 6 illustrates the streamlines picture for  $z_0 = 0.2$  mm. The indicated values of flow rate are expressed as sampling factor (1). Strong disturbances of the flame flow field for this small distance

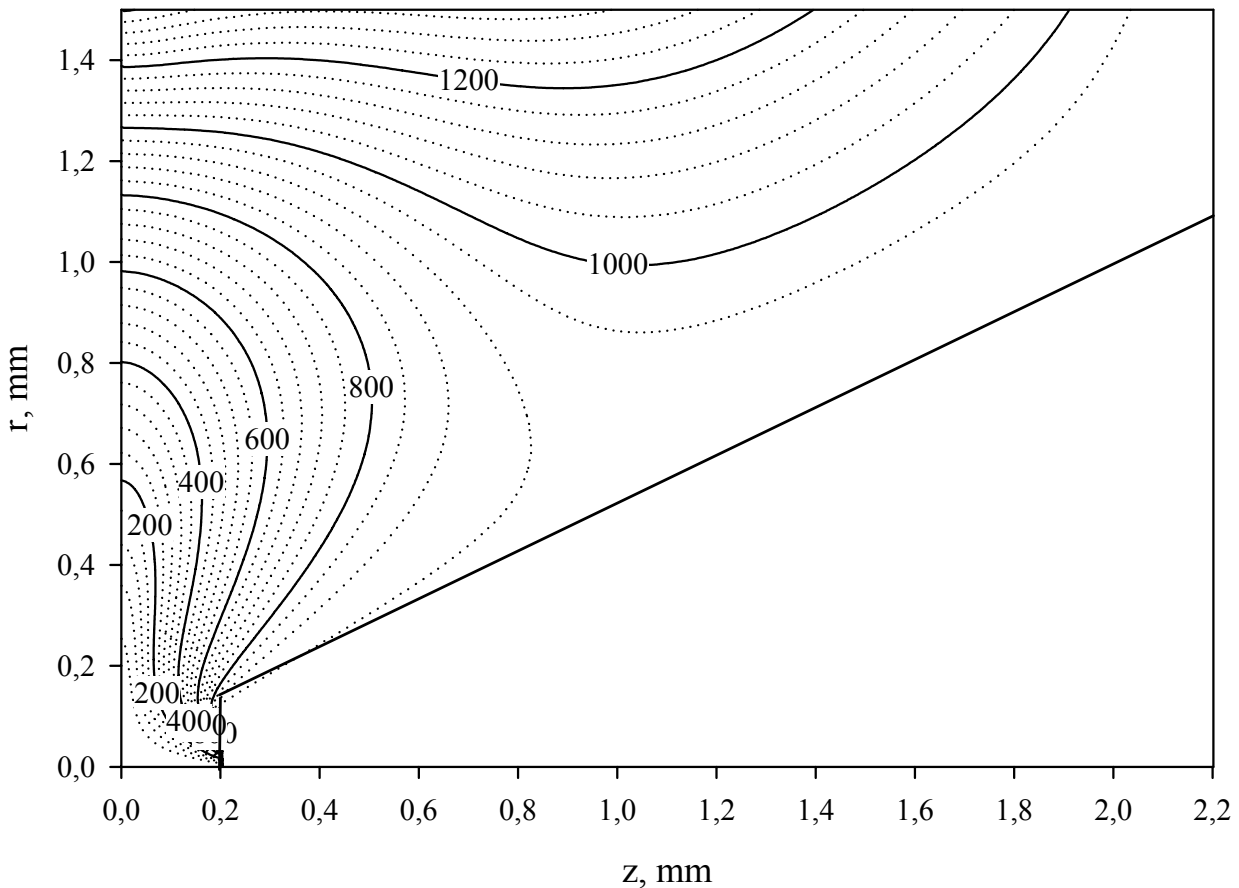


Fig. 6. Streamlines picture for  $z_0 = 0.2$  mm.

between the probe and the burner surface are evident. At some distance from the probe tip the stagnation point is formed on the probe cone surface that is typical of the considered flow [3, 4, 6]. The stagnation streamline divides the flow near the probe on two fractions, one of which reaches the probe orifice while another does not. The gas flow rate through the probe orifice that may be determined from Fig. 5 is between 920 and 940 (the exact value is  $\alpha = 925.2$ ).

The part of the above flow field with more detailed structure of the streamlines picture in the probe tip vicinity is illustrated in Fig. 7.

The streamlines picture for  $z_0 = 0.8$  mm is illustrated in Fig. 8. For this, maximum among the considered distances  $z_0$ , the flow field disturbances are noticeably smaller than for  $z_0 = 0.2$  mm (see Fig. 6). The stagnation point on the cone surface is observed again. The flow rate through the probe orifice ( $\alpha = 662.5$ ) is lower than for  $z_0 = 0.2$  mm due to higher values of temperature in the vicinity of the probe tip.

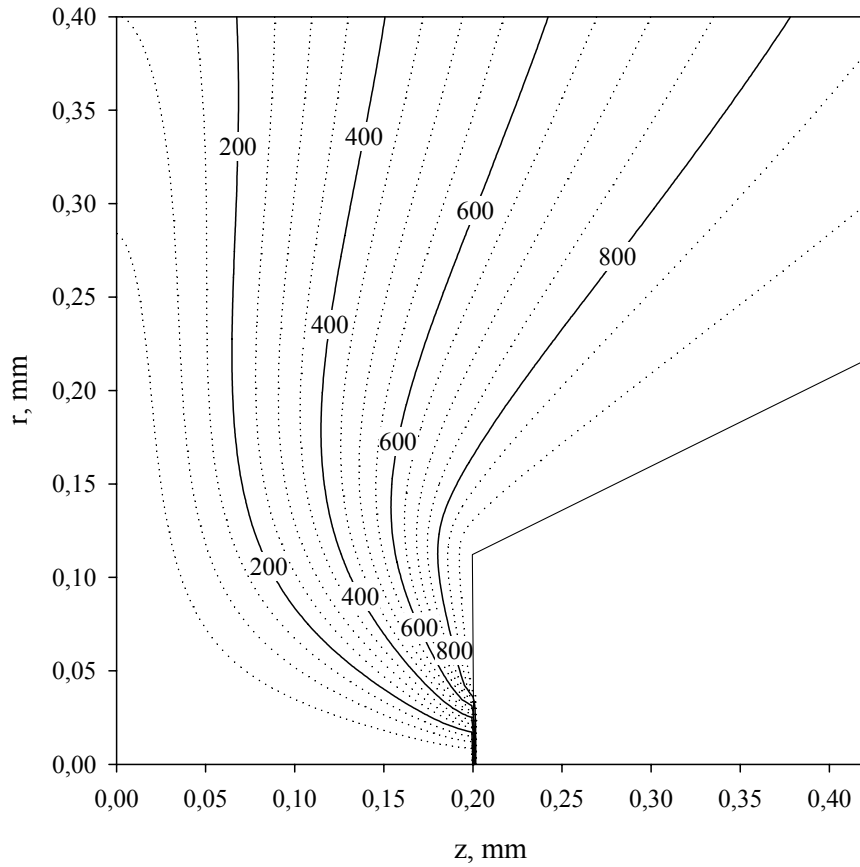


Fig. 7. Streamlines picture in the probe tip vicinity for  $z_0 = 0.2$  mm.

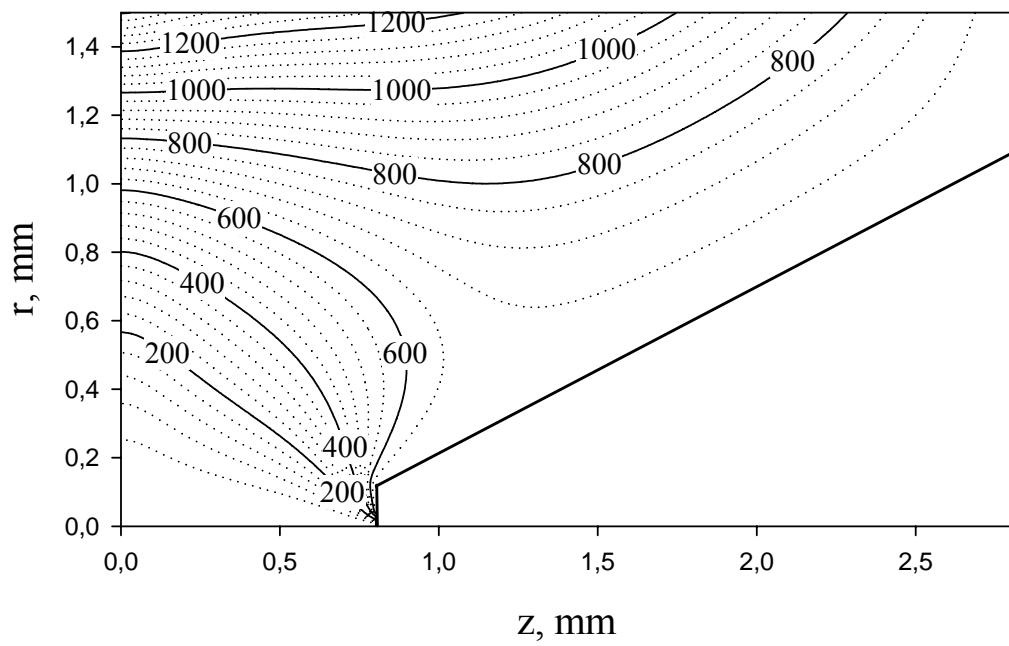


Fig. 8. Streamlines picture for  $z_0 = 0.8$  mm.

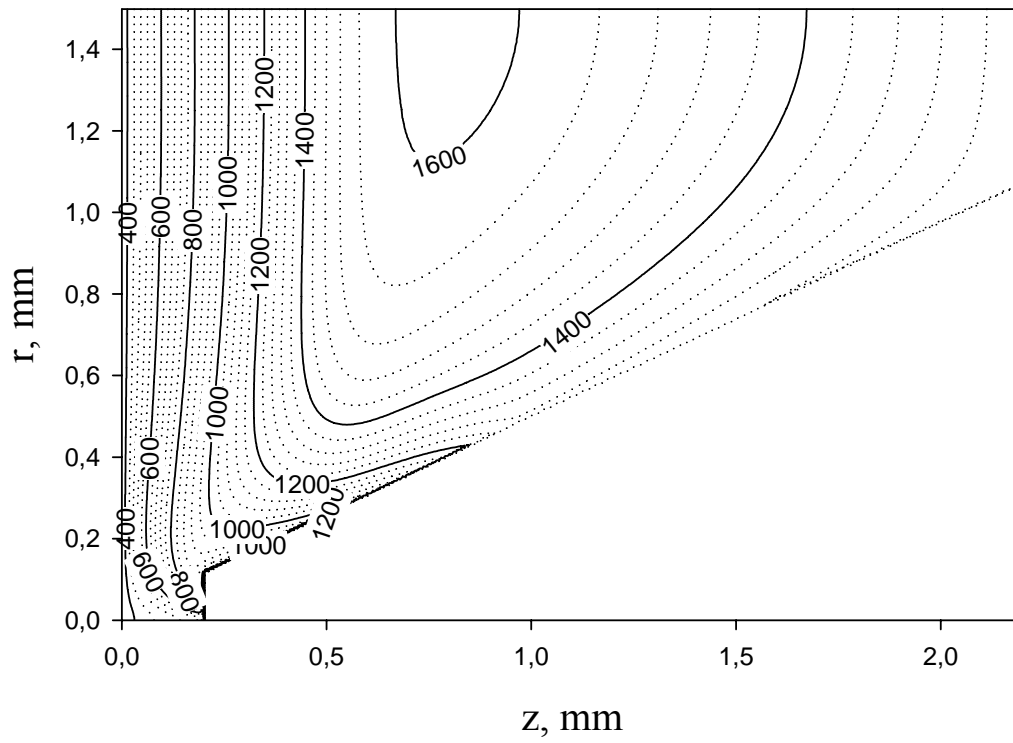


Fig. 9. Isotherms for  $z_0 = 0.2$  mm.

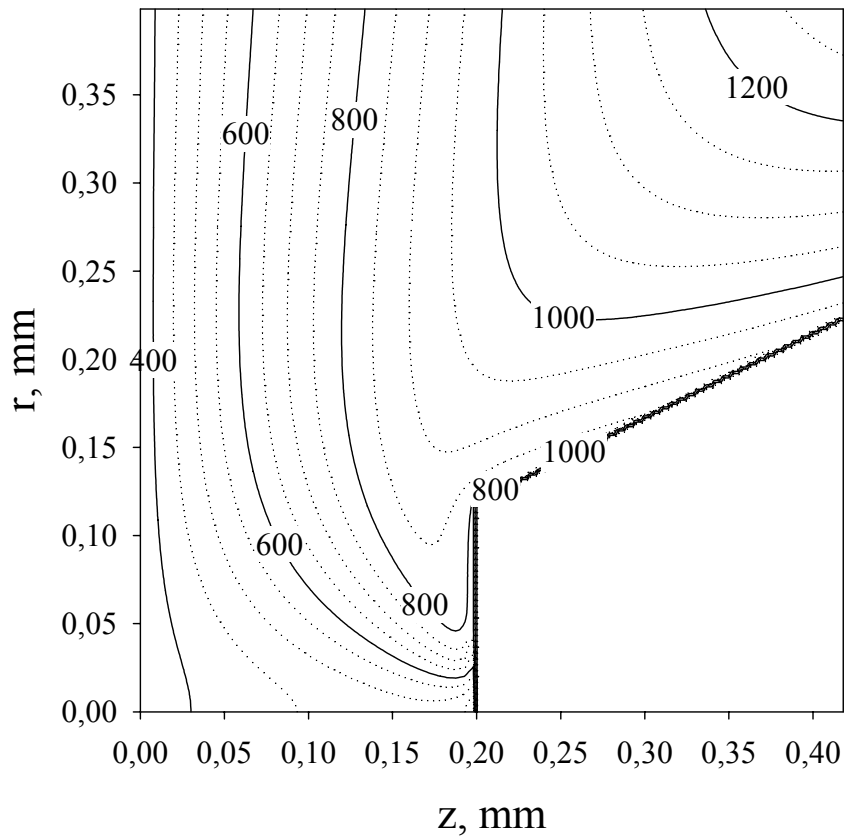


Fig. 10. Isotherms in the probe tip vicinity for  $z_0 = 0.2$  mm.

Figure 9 illustrates the field of isotherms for  $z_0 = 0.2$  mm. This picture also reveals strong disturbances of the flame flow field. The cooling effect of the flow periphery by the cone wall is well pronounced. The part of the same field in the vicinity of the probe tip is shown in Fig. 10.

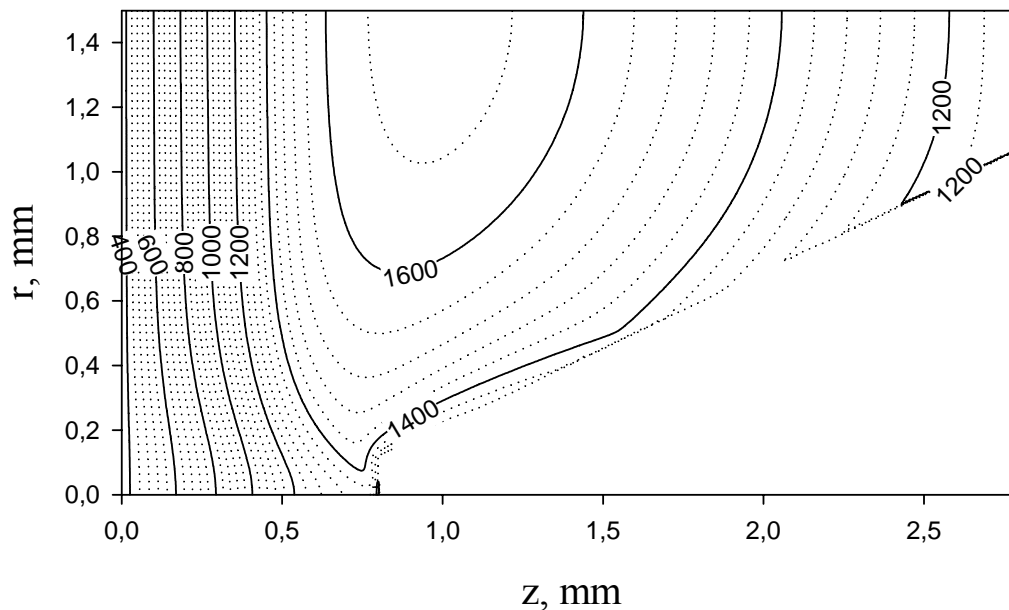


Fig. 11. Isotherms for  $z_0 = 0.8$  mm.

For complete representation of the peculiarities of the studied flow the isotherms for  $z_0 = 0.8$  mm are illustrated in Fig. 11. The disturbances of the flow field are lower than that for  $z_0 = 0.2$  mm. Again the cooling effect of periphery of the flow is observed.

Axial distribution of the parameters of the flow for  $z_0 = 0.2$  mm is illustrated in Fig. 12. The distribution of temperature in undisturbed flow is also shown for comparison.

The axial velocity monotonously increases from the value at the burner surface up to the sonic value on the probe orifice.

The pressure remains almost constant in the main part of the distance to the probe tip except its small vicinity (about 0.05 mm) where the drop of pressure by a factor about 2 takes place due to the suction effect of the probe orifice. As a consequence of such a behaviour of the pressure, the temperature and the density are almost inverse each other.

The increase of temperature with  $z$  is significantly lower than in undisturbed flame in spite of the effect of source term. This is caused by the acceleration of the flow that considerably reduces the residence time that the gas is spent inside the region with given intensity of the heat source. In the near vicinity of the probe tip even the drop of temperature caused by the acceleration of the gas here takes place.

Radial distribution of the parameters for  $z_0 = 0.2$  mm in the probe tip plane is illustrated in Fig. 13. The results are shown for the meshes that are nearest to the tip – for axial velocity these points correspond just to the tip plane, while other quantities are shown at the distance  $dz/2$  from the tip plane.

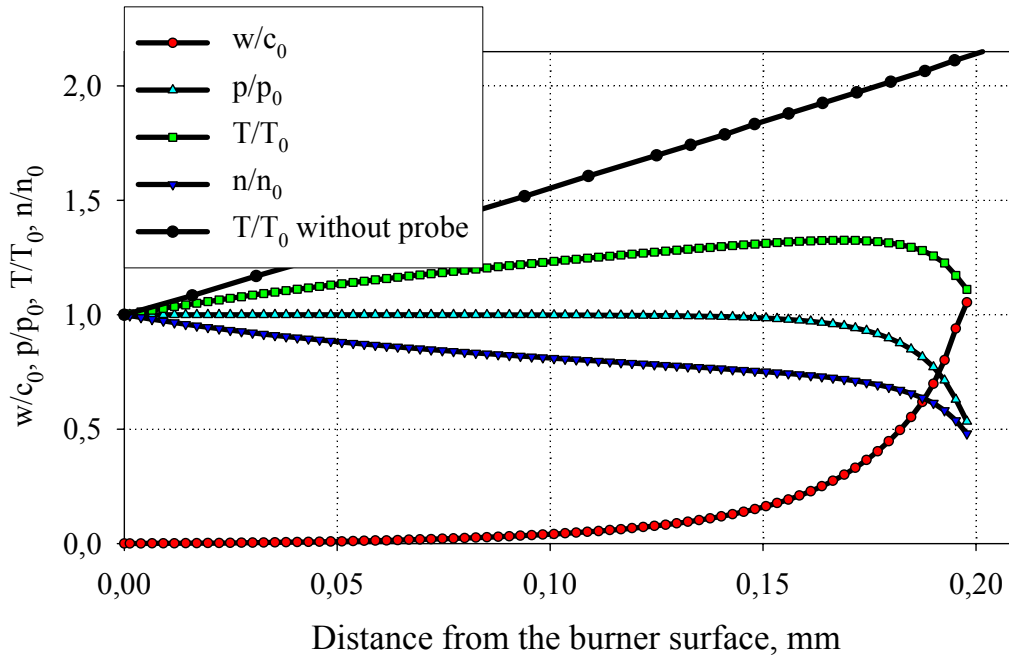


Fig. 12. Axial distribution of parameters for  $z_0 = 0.2$  mm.

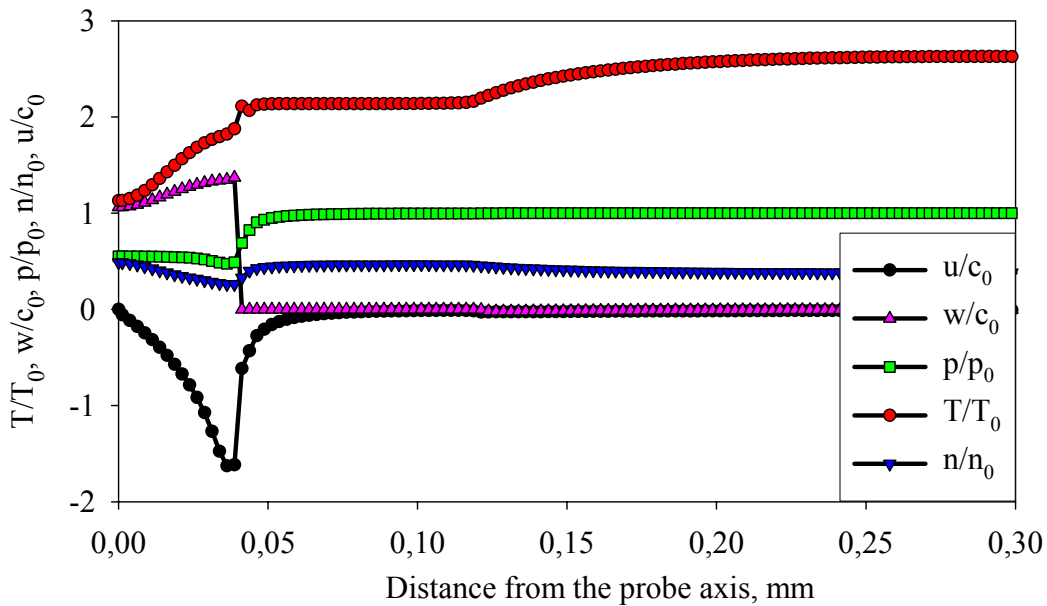


Fig. 13. Radial distribution of parameters for  $z_0 = 0.2$  mm in the probe tip plane.

The radial velocity in the region of radiuses corresponding to the probe orifice position ( $r \leq 0.04$  mm) is negative, that reflects the suction effect of the probe. In the vicinity of the orifice edge this velocity slightly exceeds the axial velocity, they both are close to the sound speed here.

The temperature increases with radius due to the weakening of the suction effect of the probe as well as due to the heat exchange with more hot peripheral parts of the flow. In the region  $0.04$  mm  $< r < 0.12$  mm, corresponding to the probe tip surface, the gas temperature is almost constant and equal to the surface temperature, while for  $r > 0.12$  mm slow increase of temperature to its value in undisturbed flow takes place.

The axial velocity for  $r \leq 0.04$  mm is of exactly sonic value due to the used boundary conditions and hence it reflects the behaviour of the temperature. In the region  $0.04$  mm  $< r < 0.12$

mm the axial velocity is zero, while for  $r > 0.12$  mm it has low negative values due to the inverse flow here (see Fig. 7).

The pressure is almost constant for all the radiuses except the region for  $r \leq 0.04$  mm where it drops by a factor about 2.

Due to the equation of states, the radial dependence of density is a consequence of considered dependencies of temperature and pressure.

The radial and axial distributions of the parameters for another distances  $z_0$  are similar to those discussed above.

Based on the distribution of the flow field gas dynamic parameters the only quantity that allows one to judge about the probe-induced distortions is the gas flow rate through the probe orifice. Figure 14 illustrates the obtained results for the sampling factor for 4 considered distances  $z_0$ . The values of  $\alpha$  at the ideal sampling from undisturbed flow calculated by isentropic relations for critical flow through the Laval nozzle are also shown in Fig. 14. The calculated data for real probe are higher than those obtained at ideal sampling. The reasons for underestimation of the flow rate at ideal sampling are quite clear – the discussed above effect of the acceleration of the flow near the real probe results in lower values of temperature in the vicinity of the probe tip in comparison with the temperature in undisturbed flame. The lower temperature leads to the higher density, and hence the higher values of the flow rate should take place in the real conditions.

The numerical results for the flow rate shown in Fig. 14 may be interpreted as being shifted downstream in comparison with those obtained at ideal sampling. Similar shift that takes place for species concentration on the flow centerline will be illustrated below.

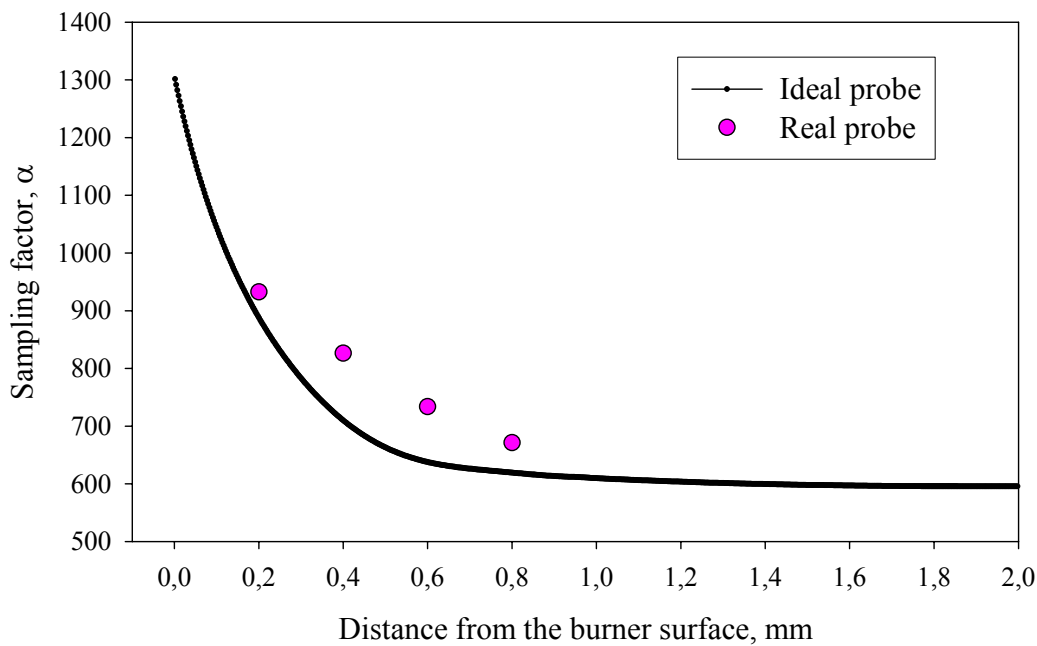


Fig. 14. Perturbation of the gas flow rate through the probe orifice.

Fig. 15 shows temperature profiles obtained numerically and experimentally. Two categories of profiles are plotted.

The first one refers to unperturbed profiles: the profile (1) is obtained by calculations using Chemkin Premix code [29] (the same as shown in Fig. 4), and the profile (2) is measured using a thermocouple without the sampling probe in the flow. As it is seen the calculated and measured data are in satisfactory agreement though some noticeable difference between them takes place.

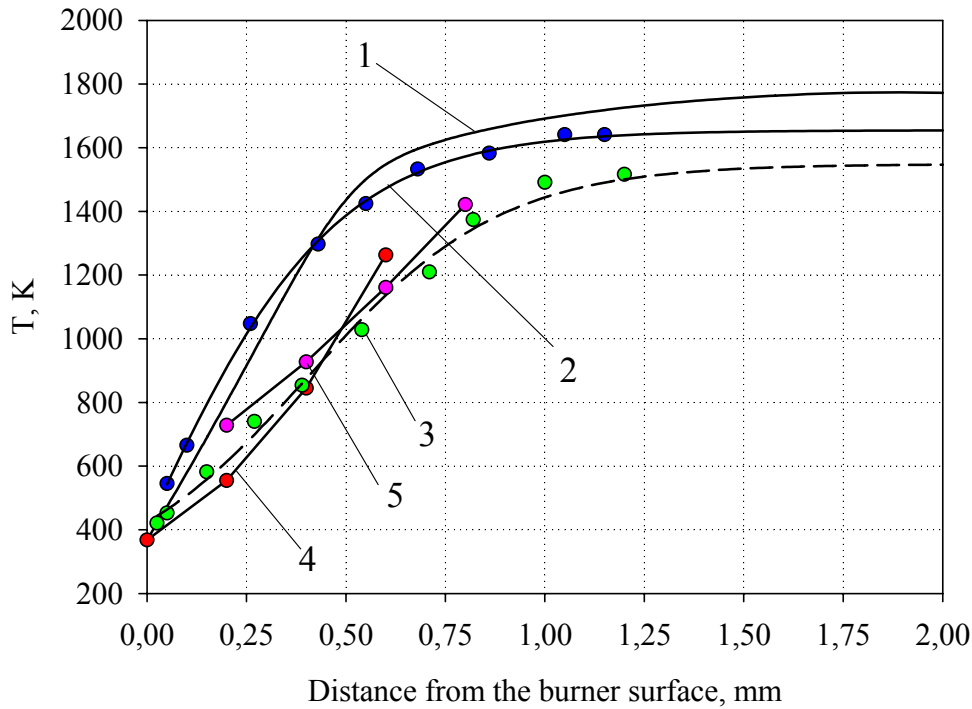


Fig. 15. Perturbation of axial distribution of temperature.

The second one refers to perturbed temperature profiles: the profile (3) is measured by the thermocouple directly in front of the probe tip at the distance of 0.2 mm from the tip, and the profile (4) corresponds to the calculated values of temperature on the flow centerline 0.2 mm upstream the probe tip for 4 considered locations of the probe in the flame. One can see that both calculated and measured perturbed profiles are shifted approximately 0.2 – 0.3 mm downstream in comparison with unperturbed temperature distribution. The calculated and measured profiles are quite similar that indicates about adequate description of the main features of the studied flow by the model.

The profile (5) plotted in Fig. 15 represents the temperature deduced from the calculated values of the gas flow rate shown in Fig. 14 by isentropic relations for critical flow through the Laval nozzle. These data may be considered as temperature “measured” by choked probe technique. As it is seen from Fig. 15, the profile (5) is also in good agreement with the results of thermocoupled measurements (Profile (4)) and reveals some similarity between the approaches used in Ref. [15] and Refs. [17 – 21] to take into account the probe-induced perturbation of the flame on the distribution of species concentration.

#### 4. CONCENTRATION DISTRIBUTION

The discussed above gas dynamic structure of the flow over the probe in the conditions similar to those in the real flame contains little information about the probe-induced perturbations of the flow from experimental point of view – the most important problem is connected with perturbations of species concentration. This problem may be clarified in the same manner that was used for gas dynamic simulation. Namely, since the main component of the considered flame is chemically neutral argon, it is possible to simulate the evolution of concentration of ever flame species in the flow field in the frames of diffusion equation for binary gas mixture of this species with argon (species 2).

The diffusion equation for axisymmetric flow of binary gas mixture has the form

$$\rho \frac{\partial c_1}{\partial t} + \rho u \frac{\partial c_1}{\partial r} + \rho w \frac{\partial c_1}{\partial z} = -\frac{1}{r} \frac{\partial}{\partial r} (r J_{1r}) - \frac{\partial}{\partial z} J_{1z}, \quad (8)$$

where  $c_1$  is the mass fraction of species 1. The diffusion fluxes  $J_{1r}$ ,  $J_{1z}$  include the concentration, pressure and thermal diffusion terms and are expressed as

$$J_{1r} = -\rho D_{12} \left[ \frac{\partial c_1}{\partial r} + \frac{m_2 - m_1}{m} c_1 (1 - c_1) \frac{\partial \ln p}{\partial r} + \frac{m_1 m_2}{m^2} k_T \frac{\partial \ln T}{\partial r} \right],$$

$$J_{1z} = -\rho D_{12} \left[ \frac{\partial c_1}{\partial z} + \frac{m_2 - m_1}{m} c_1 (1 - c_1) \frac{\partial \ln p}{\partial z} + \frac{m_1 m_2}{m^2} k_T \frac{\partial \ln T}{\partial z} \right],$$

where  $D_{12}$  is the binary diffusion coefficient,  $m_1$ ,  $m_2$  - molecular masses of species 1 and 2,  $m$  - the mean molecular mass,  $k_T$  - thermal diffusion ratio.

The diffusion equation was solved using the same staggered grid and finite-difference scheme as in gas dynamic simulation, the concentration being determined in the center of the cell. Four species of the flame components were considered – CH<sub>4</sub>, CO<sub>2</sub>, H<sub>2</sub>O and O<sub>2</sub>, though the approach may be applied to analyze the evolution of concentration of ever species of the flame. For approximate accounting for the effect of chemical reactions the source term  $Q_{source}$  was introduced in the diffusion equation providing the given distribution of concentration of considered species in undisturbed flame. This term depending only on  $z$  was obtained from the relation written in non-dimensional form in the same manner as it was made in § 2.4 for energy equation

$$\frac{\partial c_1}{\partial t} = Q_{conv} + Q_{diff} + Q_{source} = 0, \quad (9)$$

where the convective term entering the diffusion equation (8) is schematically denoted as  $Q_{conv}$  while the diffusion term is denoted as  $Q_{diff}$ . The finite-difference representation of the relation (9) for one-dimensional flow was made on the same staggered grid for axial coordinate as in two-dimensional calculations, the values of source term being determined in the center of the cell. The distributions of temperature, density and axial velocity in the flow were set in the same manner as it was made in § 2.4 during the calculations of the source term for energy equation. The distribution of molar concentration of considered species was set in accordance with the results of simulation of undisturbed flame flow by Chemkin Premix code [29]. These distributions are illustrated in Fig. 16 (it should be noted that in the frames of the approach applied here all other components of the flame are replaced by argon molecules). The temperature dependence of  $\rho D_{12}$  and  $k_T$  for considered binary mixtures was assumed to be described by Lennard-Jones (6 – 12) potential [31] with parameters  $\sigma = 3.746 \text{ \AA}$ ,  $\varepsilon/k = 141.4 \text{ K}$  for CH<sub>4</sub>,  $\sigma = 3.763 \text{ \AA}$ ,  $\varepsilon/k = 244 \text{ K}$  for CO<sub>2</sub>,  $\sigma = 2.605 \text{ \AA}$ ,  $\varepsilon/k = 572.4 \text{ K}$  for H<sub>2</sub>O and  $\sigma = 3.458 \text{ \AA}$ ,  $\varepsilon/k = 107.4 \text{ K}$  for O<sub>2</sub> and commonly used combination rules to describe the interaction between unlike molecules [31].

The obtained axial dependencies of  $Q_{source}(z)$  for considered species are illustrated in Fig. 17. Positive values take place for combustion products CO<sub>2</sub> and H<sub>2</sub>O while negative values – for reagents CH<sub>4</sub> and O<sub>2</sub>. Since the undisturbed flame is isobaric the pressure diffusion does not contribute to the diffusion flux and hence to the value of  $Q_{source}$ . The contribution of thermal diffusion is non-zero but small, as it can be seen from Fig. 17, where for each species the source term is calculated with (CD and TD) and without taking into account the contribution of thermal diffusion (CD only).

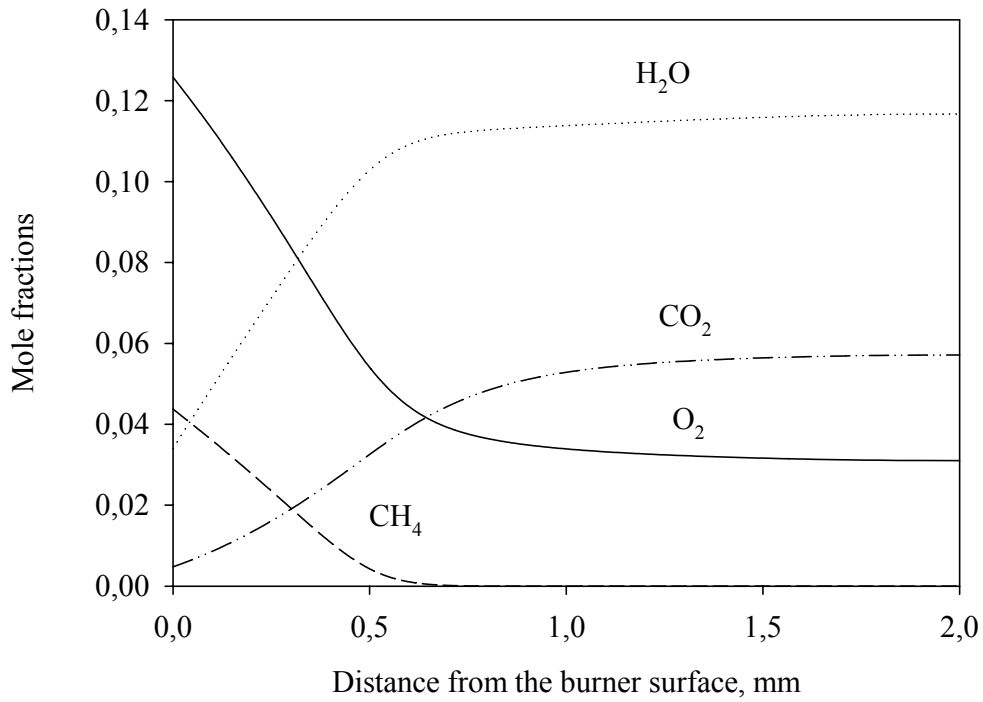


Fig. 16. The distribution of concentrations in undisturbed flame.

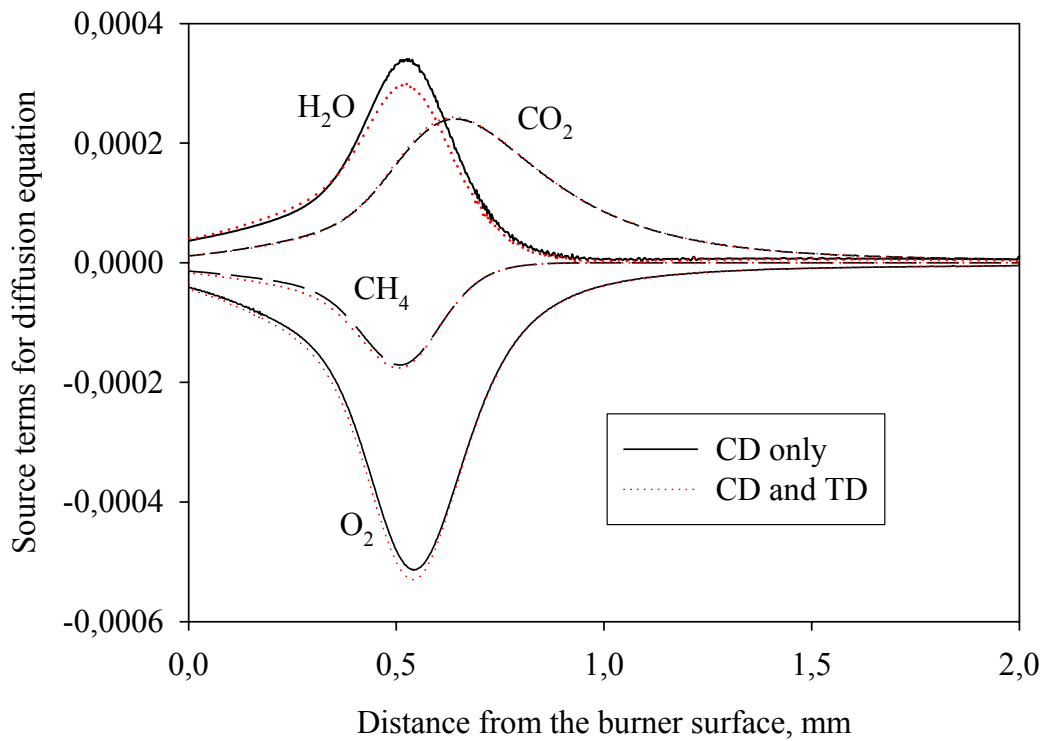


Fig. 17. The source terms for diffusion equation.

As it was mentioned above, the diffusion equation completed by source term was solved using the same staggered grid and finite-difference scheme as in gas dynamic simulation. The problem was treated in a linear statement, i. e. without taking into account the effect of diffusion on the flow field parameters. The boundary conditions for diffusion equation were set as follows.

At the burner surface (line 1 – 7, see Fig. 1) the concentration was prescribed to be the same as in undisturbed flame.

At the solid boundaries (lines 3-4-5) the absence of the diffusion flux was assumed.

At the probe orifice surface (line 2 - 3) and at the upper permeable boundary (line 7 – 6) the concentration is specified by extrapolation from internal points of the domain.

At the axis of symmetry (line 1 – 2) the radial derivative of concentration is prescribed to be zero.

Finally, at the solid boundary (5 – 6) the concentration was prescribed to be the same as behind the flame front.

The simulations show that the effects of pressure and thermal diffusion on concentration distribution in the flow field are small. We will not illustrate these effects taking into account the approximate nature of the model. The results presented below were obtained with accounting for concentration diffusion only.

Figure 18 illustrates the axial distributions of methane mole fraction. The corresponding distribution in undisturbed flame is also shown for comparison. As can be seen from these results, for all four values of  $z_0$  the decrease of  $\text{CH}_4$  concentration with  $z$  is significantly lower than in

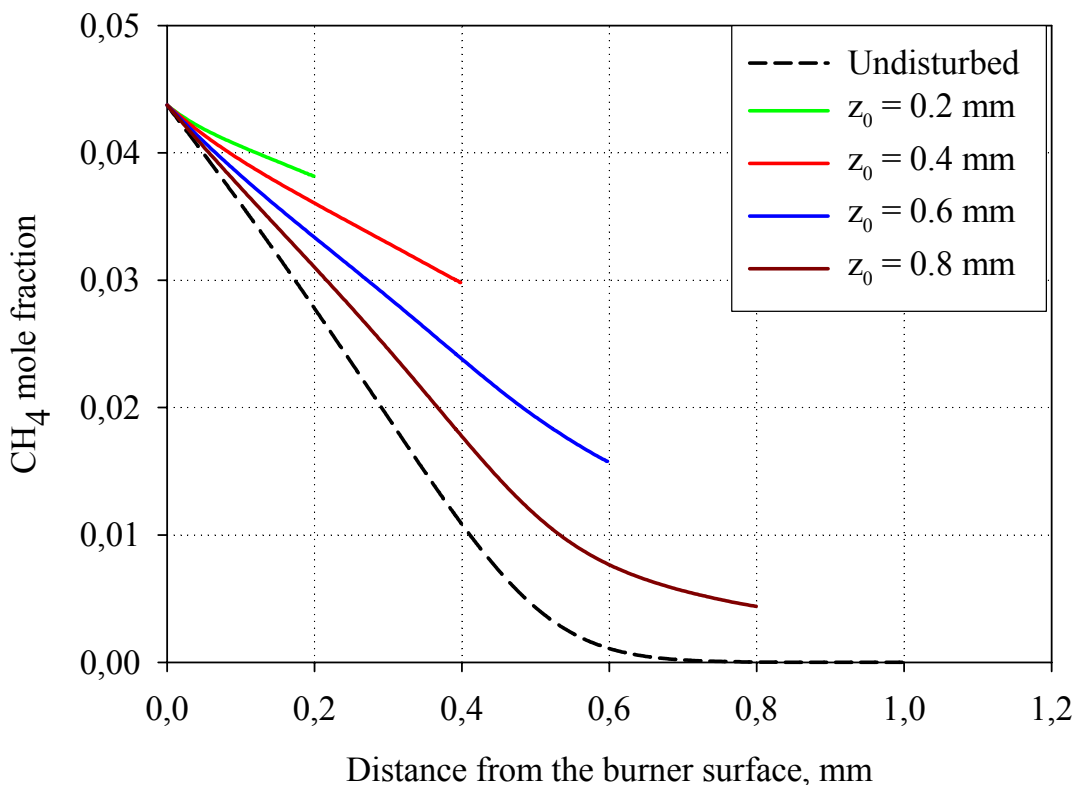


Fig. 18. Axial distributions of methane mole fraction.

undisturbed flame in spite of the effect of source term. This is caused by the acceleration of the flow that considerably reduces the residence time that the gas is spent inside the region with given intensity of the sink source. The concentrations in the probe orifice center, representing the most interest from experimental point of view, are shifted downstream in comparison with the position of

the same concentration in undisturbed flame. The comparison of these distributions with axial distribution of temperature (see Fig. 12) indicates about their qualitative analogy and reflects the

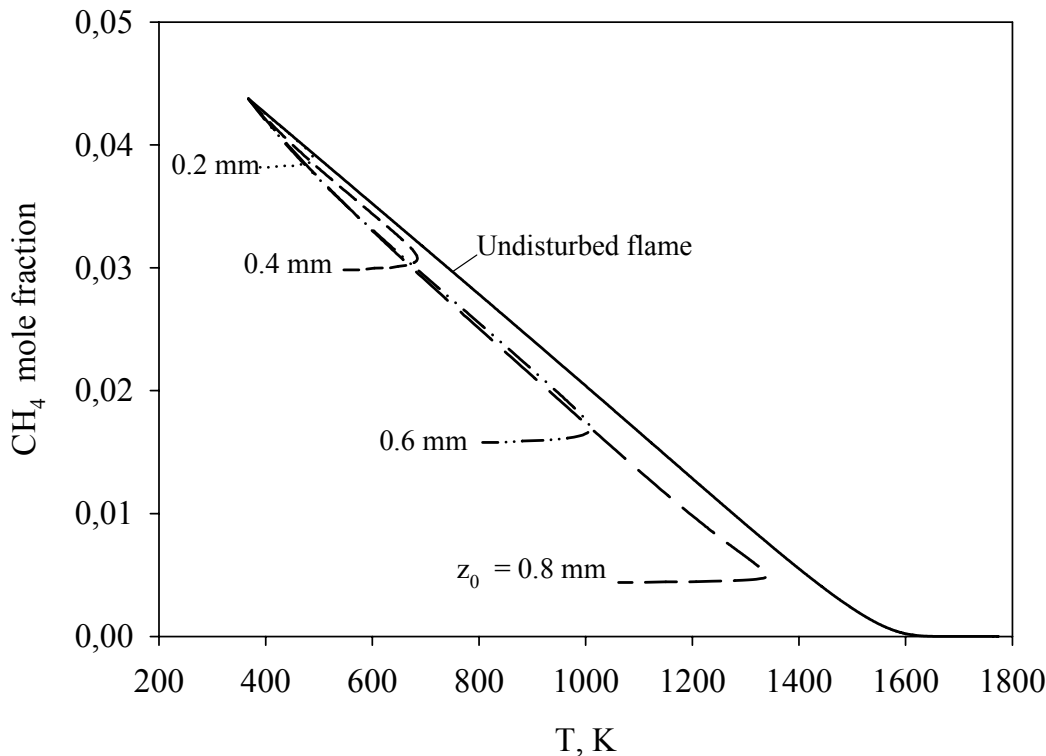


Fig. 19. The relation between methane mole fraction and temperature in undisturbed flame and on the centerline of disturbed flow for different locations of the probe in the flame.

known similarity between heat- and mass-transfer processes.

The degree of this similarity is well illustrated in Fig. 19 where the methane mole fraction on the centerline of the flow is plotted against the local temperature for 4 considered locations of the probe in the flame. The same dependence for undisturbed flame flow is also shown for comparison. The analysis of these data reveals an important feature of the flame flow perturbed by the sampling – the relation between local values of concentration and temperature on the centerline of perturbed flow is very close to that in unperturbed flame. This rule violates only in small vicinity of the probe orifice where rapid decrease of temperature due to high acceleration of transonic flow takes place (see Figs. 12, 19). These results allows one to explain the good agreement between measured and calculated concentrations obtained in Ref. [15, 17 – 21], mentioned in the introduction.

The axial distributions of concentrations of another considered species reveal the same feature as shown in Figs. 18 and 19.

The undisturbed flame is plane and one-dimensional, therefore no transverse gradients of parameters should effect the concentration distribution. As it was illustrated above the flow near the probe tip is characterized by strong radial gradients of parameters (see Fig. 13). In this respect it is interesting to clarify the effect of radial diffusion flux on the concentration distribution flow field. This problem can not be resolved experimentally but it is possible to solve it numerically simply neglecting the value  $J_{1,r}$  in Eq. 8.

Figure 20 illustrates the axial distributions of  $\text{CO}_2$  mole fraction for  $z_0 = 0.8$  mm obtained with and without accounting for radial diffusion flux. The significant effect of  $J_{1,r}$  on concentration

distribution is evident. Similar conclusion can be derived from radial distributions of concentration in the probe tip plane shown in Fig. 21 for the same regime. Highly non-uniform transverse

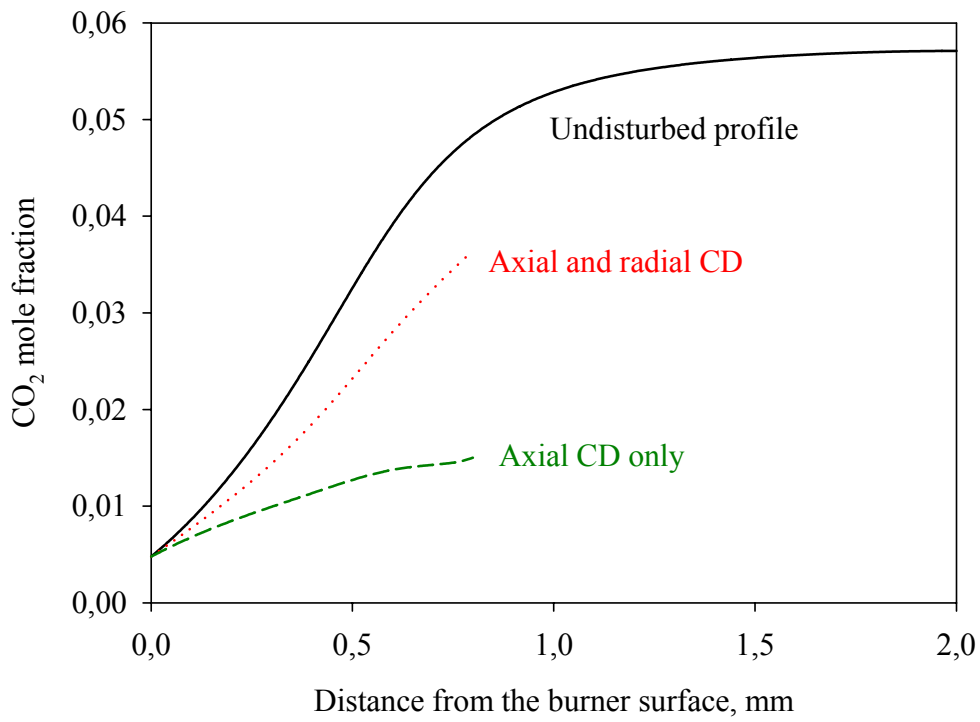


Fig. 20. The effect of radial diffusion flux on axial distribution of CO<sub>2</sub> mole fraction for  $z_0 = 0.8$  mm.

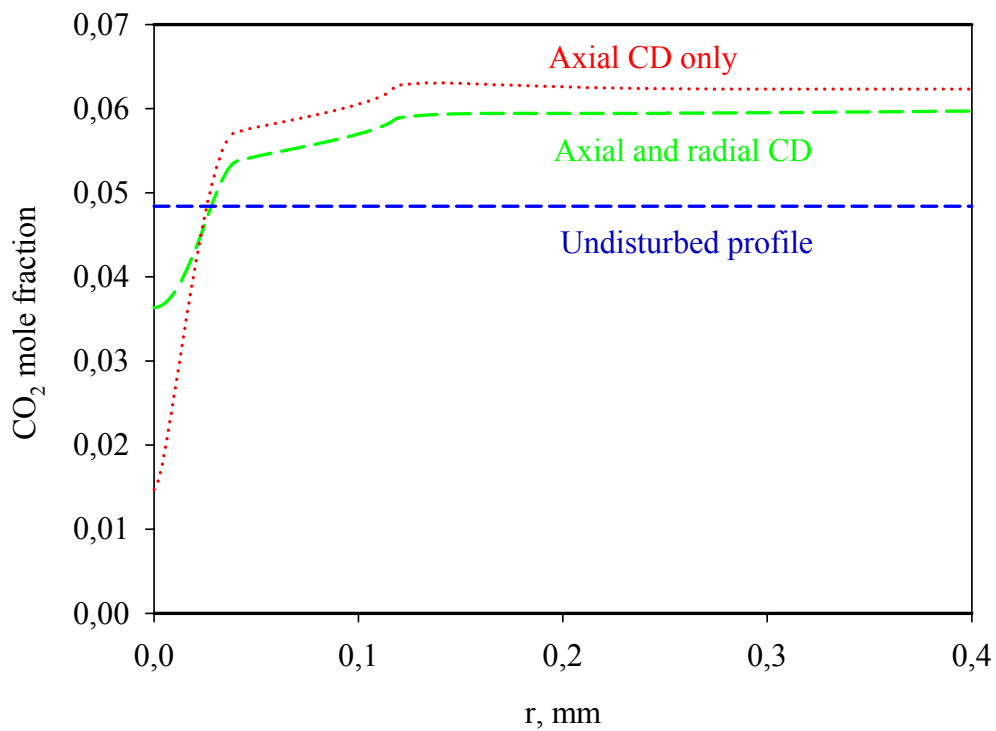


Fig. 21. The effect of radial diffusion flux on radial distribution of CO<sub>2</sub> mole fraction in the probe tip plane for  $z_0 = 0.8$  mm.

distribution of concentration caused by different evolution of the parameters along the streamlines, observed for  $J_{1r} = 0$ , becomes significantly smoothed with accounting for radial diffusion flux.

Based on the conservative nature of the pressure in axial distribution of parameters illustrated above (see Fig. 12), at the earlier stage of this study an idea to simulate the mixture composition on the axis of the real flame by Chemkin Premix code [29] (which operates with isobaric conditions) by specifying the streamtube area on the flow axis was considered. In this case it will be possible to calculate the probe-perturbed concentrations in the vicinity of the probe tip in the exact quasi-one-dimensional statement. The illustrated above strong effect of radial diffusion flux makes this idea useless.

As it is seen from Fig. 21, the difference between the perturbed concentration and unperturbed one on the same distance from the burner has different sign at the centerline and at the periphery of the flow. This peculiarity of radial distribution of concentration in the probe tip plane takes place for all of the considered regimes and is caused by different evolution of the parameters along the different streamlines and the reverse flow along the probe cone surface near the probe tip (see Figs. 6 – 8) resulting in sampling of gas from both downstream and upstream of the probe [15]. Similar relation between disturbed and undisturbed concentration was found in Ref. [3] where the concentration evolution was treated as self-diffusion process in more simple gas dynamic model of the flow.

Due to the discussed radial gradient of concentration in the probe tip plane the measured mixture composition would depend on experimental procedure. In typical molecular beam system when only small near axial part of the sample reaches the detector the results would reflect the concentration distribution on the axis of the flow. In the molecular leakage experiments when the total gas flow rate through the probe orifice is analyzed the obtained results would correspond to the radially averaged value of concentration over the probe orifice. As can be seen from Fig. 21 the

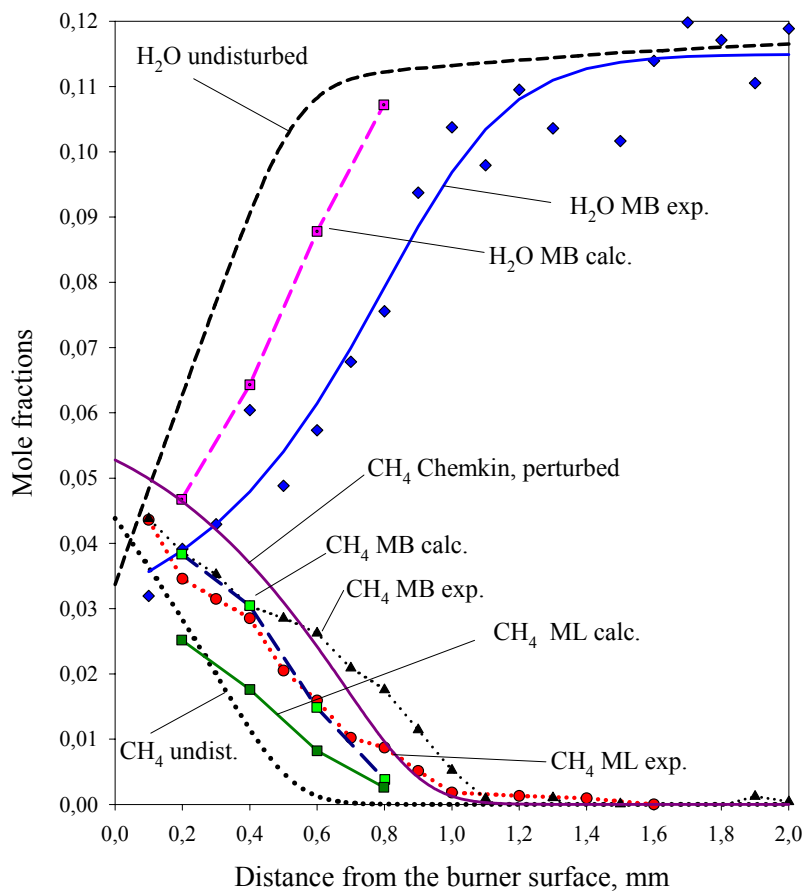


Fig. 22. Axial distributions of CH<sub>4</sub> and H<sub>2</sub>O concentrations.

latter procedure would give the results with less deviation from undisturbed concentration in comparison with molecular-beam experiment.

The above stated conclusion is well confirmed by direct comparison between calculated and measured concentration profiles of CH<sub>4</sub> and H<sub>2</sub>O shown in Fig. 22. The results obtained in molecular-beam experiments are denoted as MB, while those obtained in molecular leakage experiments are denoted as ML. The calculated results denoted as MB correspond to the values of concentration in the probe orifice center, while those denoted as ML (for CH<sub>4</sub>) were obtained by averaging the radial flux of methane over the probe orifice based on the calculated radial distributions of density, axial velocity and CH<sub>4</sub> concentration. The profiles of CH<sub>4</sub> and H<sub>2</sub>O in unperturbed flame are also shown for comparison.

CH<sub>4</sub> concentration profile calculated by Chemkin Premixed code [29] on the basis of fixed temperature profile measured by a thermocouple in front of the probe tip at the distance of 0.2 mm from the tip (curve 3 in Fig. 15), i. e. in the frames of the same approach as was used in Refs. [17 – 21], is also plotted in Fig. 22 and denoted as “CH<sub>4</sub> Chemkin, perturbed”. These data are in better agreement with the data obtained in molecular-beam experiment in comparison with the profile calculated by the model (CH<sub>4</sub> MB calc.).

As it is seen from Fig. 22 both measured and calculated “MB” profiles are shifted downstream in comparison with unperturbed ones, the experimental values of shift are higher than calculated ones by factor about 2. The shift of “ML” profiles of CH<sub>4</sub> is noticeably lower than “MB” ones, moreover, the calculated “ML” profile is negative at  $z_0 = 0.2$  mm.

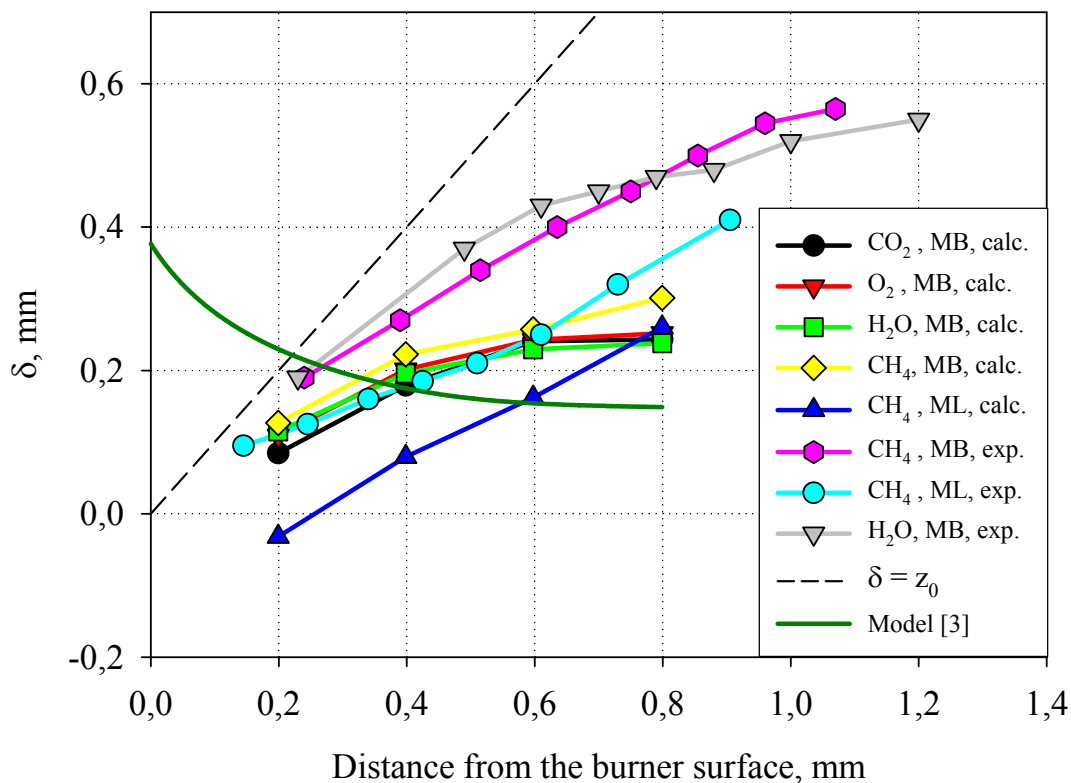


Fig. 23. Values of shift for species concentration profiles compared to unperturbed ones.

All the obtained data for values of shift  $\delta$  are summarized in Fig. 23, the data being denoted in the same manner as in Fig. 22. The prediction of the approximate model available in literature [3] is also shown for comparison (The data for  $\delta$  were calculated by relation (2) for sonic flow in the probe orifice plane, the flow parameters being connected with those in unperturbed flow by isentropic relations. The diffusion coefficient entering the relation (2) was used for CH<sub>4</sub> – Ar mixture. The values of  $\delta$  for other of considered mixtures slightly differ from those plotted in Fig.

23 due to the difference in diffusion coefficients). The dotted line ( $\delta = z_0$ ) shows maximum possible value of shift for given distance  $z_0$  between the probe tip and the burner surface. As it was mentioned earlier, the calculated values of shift (for “MB” data) are systematically lower than the measured ones by factor about 2 that may be connected with nonlinear effect of flow perturbation on the kinetics of chemical reactions. This effect can not be taken into account by the developed model with spatially fixed sources of energy and concentrations. As it is seen from Fig. 23 the approximate relation for shift available in literature [3] may be used only for estimation of its order of magnitude. This relation predicts the decrease of shift with increasing the distance between the probe tip and the burner that is opposite to the results of observations. Moreover, at small distances  $z_0$  the corresponding predictions ( $\delta > z_0$ ) have no physical sense.

## CONCLUSION

The main results of the performed study may be summarized as follows:

1. Based on the Navier-Stokes equations completed by source terms for energy and diffusion equations the numerical model for the flame flow near the sampling probe counting for the effects of chemical reactions is developed.
2. The simulation of the external flow near the probe with orifice diameter 80  $\mu\text{m}$ , tip diameter 240  $\mu\text{m}$  and half-angle of conical part of the probe  $25.5^\circ$  for the methane-oxygen-argon flame stabilized on the flat burner at atmospheric pressure is performed. The boundary conditions for temperature on the probe surface were specified on the basis of thermocoupled measurements.
3. Using thermocouple technique temperature profiles in unperturbed and perturbed flames are measured. For temperature measurements in perturbed flame the thermocouple was located at the distance of 0.2 mm from the probe tip. The shift of the perturbed profile towards the unperturbed one is determined.
4. Concentration profiles of major stable species in the flame are measured using molecular-beam sampling system as well as molecular leakage sampling system coupled with mass-spectrometer. The experimental results are compared with modeling data obtained using Chemkin Premix code for unperturbed flame and with numerical results for perturbed flame. The values of shift for concentration profiles of major species in perturbed flame compared to the same unperturbed profiles are determined.
5. The results of measurements of temperature in perturbed flow are in satisfactory agreement with calculated temperature on the flow centerline at the point 0.2 mm upstream the tip, that indicates about adequate description of the main features of the studied flow by the model.
6. The temperature deduced from the calculated values of the gas flow rate through the probe orifice by the relation for choked probe technique is in good agreement with the results of thermocoupled measurements that reveals some similarity between the approaches used in Ref. [15] and Refs. [17 – 21] to take into account the probe-induced perturbation of the flame on the distribution of species concentration.
7.  $\text{CH}_4$  concentration profile calculated by Chemkin Premixed code on the basis of fixed temperature profile measured by a thermocouple in front of the probe tip at the distance of 0.2

mm from the tip, i. e. in the frames of the same approach as was used in Refs. [17 – 21], is in fairly good agreement with the data obtained in molecular-beam experiment.

8. The developed model of perturbed flame predicts the downstream shift of the main flow characteristics (temperature on the flow centerline, gas flow rate through the probe orifice, species concentrations in the probe orifice center, etc.) in comparison with those in unperturbed flame. The indicated feature is typical of perturbed flame flow.
9. The values of shift for concentrations are approximately the same for considered flame components ( $\text{CH}_4$ ,  $\text{H}_2\text{O}$ ,  $\text{CO}_2$ ,  $\text{O}_2$ ), that reveals the correspondence between perturbed mixture composition and unperturbed one at some point of the flame front. The values of shift increase with increasing the distance between the probe tip and the burner that is in agreement with experimental data, though the measured values of shift are higher than the calculated ones by factor about 2.
10. In accordance with the predictions of the model the methane concentration near the burning surface in perturbed and unperturbed flames are close. This conclusion seems to be important for application the probing technique for condensed system flame structure study.
11. The known peculiarity of transverse distribution of concentration in the probe orifice plane [3] when the difference between the perturbed concentration and unperturbed one on the same distance from the burner has different sign at the centerline and at the periphery of the flow is well reproduced by the model. The resulting smaller shift for methane concentration obtained in molecular leakage experiments in comparison with that obtained in molecular-beam experiment is also reproduced by the model.
12. The relation between local values of concentration and temperature on the centerline of perturbed flow is close to that in unperturbed flame. This rule violates only in small vicinity of the probe orifice where rapid decrease of temperature due to high acceleration of transonic flow takes place. These results allows one to explain the good agreement between measured by the probe and calculated concentrations obtained in widely used approach to validate detailed flame reaction mechanism in which the measured temperature profile in perturbed flame is used for modeling [15, 17 – 21].
13. The approximate relation for shift available in literature [3] may be used only for estimation of its order of magnitude. This relation predicts the decrease of shift with increasing the distance between the probe tip and the burner that is opposite to the results of observations. Moreover, at small distances  $z_0$  the corresponding predictions ( $\delta > z_0$ ) have no physical sense.
14. The simulations reveal significant effect of radial diffusion fluxes on the formation of distribution of mixture concentrations in the probe orifice plane. The effect of pressure- and thermal diffusion on the concentration distribution is relatively small.

In the further version of the model instead of introducing the spatially fixed source terms into energy and diffusion equations we plan to treat the flow taking into account the simple model for chemical kinetics like Zel'dovich model or Global Kinetics approach. This refining of the model will provide the description of the nonlinear effect of gas dynamic perturbation on chemical kinetics that seems to eliminate the main reason for the observed disagreement between the model predictions and experimental results.

To clarify the effect of the boundary conditions on the probe orifice surface on the flow field we also plan to include the internal part of the probe tract in the domain of simulation. We do not expect, however, any significant changes in the results caused by this refining of the model.

## REFERENCES

1. Rosen P. Potential Flow of a Fluid into a Sampling Probe // Johns Hopkins Univ. Appl. Phys. Lab. Rept. CF-2248, Silver Spring, Md, 1954.
2. Dubinin V.V., Kolesnikov B.Ya., and Ksandopulo G.I. About Correctness of Probe Sampling from Flames // *Fizika Goreniya i Vzryva*, Vol. 13, No. 6, 1977, pp. 920 – 924 (in Russian).
3. Yi A.C., and Knuth E.L. Probe-Induced Concentration Distortions in Molecular-Beam Mass-Spectrometer Sampling // *Combustion and Flame*, Vol. 63, 1986, pp. 369 – 379.
4. Smith O.I. Probe-Induced Distortions in the Sampling of One-Dimensional Flames // *Combustion and Flame*, Vol. 40, 1981, pp. 187 – 199.
5. Hayhurst A.N., and Telford N.R. Mass Spectrometric Sampling of Ions from Atmospheric Pressure Flames-I: Characteristics and Calibration of the Sampling System // *Combustion and Flame*, Vol. 28, 1977, pp. 67 – 80.
6. Hayhurst A.N., Kittelson D.B., and Telford N.R. Mass Spectrometric Sampling of Ions from Atmospheric Pressure Flames-II: Aerodynamic Disturbance of a Flame by the Sampling System // *Combustion and Flame*, Vol. 28, 1977, pp. 123 - 135.
7. Hayhurst A.N., and Kittelson D.B. Mass Spectrometric Sampling of Ions from Atmospheric Pressure Flames-III: Boundary Layer and Other Cooling of the Sample // *Combustion and Flame*, Vol. 28, 1977, pp. 137 – 143.
8. Yoon S., and Knuth E.L. Experimental Study of Probe-Induced Distortions in Molecular-Beam Mass-Spectrometer Sampling from Flames. *Rarefied Gas Dynamics, Proc. 12th Intern. Symp.*, Edited by S.S.Fisher, Progress in Astronautics and Aeronautics, Vol. 74, Part II, N. Y., 1980, pp. 867 – 881.
9. Hartlieb A.T., Atakan B., and Kohse-Höinghaus K. Effects of a Sampling Quartz Nozzle on the Flame Structure of a Fuel-Rich Low-Pressure Propene Flame // *Combustion and Flame*, Vol. 121, No. 4, 2000, pp. 610 – 624.
10. Korobeinichev O.P., Tereshchenko A.G., Emel'yanov I.D., Kuibida L.V., Mavliev R.V., Kutsenogii K.P., Rudnitskii A.L., Fedorov S.Yu., Ermolin N.E., and Fomin V.M. Probe Mass-Spectrometry for Condensed System Flames Having Narrow Combustion Zones // Novosibirsk, Institute of Chemical Kinetics and Combustion, Preprint No. 14, 1985, pp. 37 (in Russian).
11. Biordi J.C., Lazarra C.P., and Papp J.F. Molecular Beam Mass Spectrometry Applied to Determining the Kinetics of Reactions in Flames. 1. Empirical Characterization of Flame Perturbation by Molecular Beam Sampling Probes // *Combustion and Flame*, Vol. 23, No. 1, 1974, pp. 73 – 82.
12. Emel'yanov I.D., Korobeinichev O.P., Tereshchenko A.G., and Kuibida L.V. Heat Transfer between Flame and Probe in Mass-Spectrometric Research on Flame Structure // *Combustion, Explosion and Shock Waves*, Vol. 22, No. 2, 1986, pp. 168 – 175.
13. Fristrom R.M., and Westenberg A.A. *Flame Structure*. McGraw-Hill, New York, 1965.
14. Kaiser E.W., Wallington T.J., Hurley M.D., Platz J., Curran H.J., Pitz W.J., and Westbrook S.K. Experimental and Modeling Study of Premixed Atmospheric-Pressure Dimethyl Ether-Air Flames // *J. Phys. Chem. A*, Vol. 104, 2000, pp. 8194 – 8206.
15. Nogueira M.F.M., and Fisher E.M. Effects of Dimethyl Methylphosphonate on Premixed Methane Flames // *Combustion and Flame*, Vol. 132, 2003, pp. 352 – 363.
16. Smith O.I., and Chandler D.W. An Experimental Study of Probe Distortion to the Structure of One-Dimensional Flames // *Combustion and Flame*, Vol. 63, No. 1, 1986, pp. 19 – 29.
17. Musick M., Van Tiggelen P.J., and Vandooren J. Experimental Study of the Structure of Several Fuel-Rich Premixed Flames of Methane, Oxygen, and Argon // *Combustion and Flame*, Vol. 105, 1996, pp. 433 – 450.

18. Bastin E., Delfau J.-L., Reuillon M., Vovelle C., and Warnatz J. Experimental and Computational Investigation of the Structure of a Sooting C<sub>2</sub>H<sub>2</sub>-O<sub>2</sub>-Ar Flame // Twenty-Second Symposium (International) on Combustion, The Combustion Institute, Pittsburgh, 1989, p. 313.
19. Korobeinichev O.P., Shvartsberg V. M., Shmakov A.G., Bolshova T.A., Jayaweera T.M., Melius C. F., Pitz W.J., Westbrook C.K., and Curran H. Flame Inhibition by Phosphorus-Containing Compounds in Lean and Rich Propane Flames // Proceedings of the Combustion Institute (Editors: Barlow R.S., Colket M.B., Chen J.H., Yetter R.A.), Elsevier, 2004, Vol. 30, No. 2, pp. 2350 - 2357.
20. Korobeinichev O.P., Shvartsberg V.M., Ilyin S.B., Chernov A.A., and Bolshova T.A. Laminar Flame Structure in a Low-Pressure Premixed H<sub>2</sub>/O<sub>2</sub>/Ar Mixture // Combustion, Explosion, and Shock Waves, Vol. 35, No. 3, 1999, pp. 239 - 244.
21. Korobeinichev O.P., Ilyin S.B., Bolshova T.A., Shvartsberg V.M., and Chernov A.A. The Destruction Chemistry of Organophosphorus Compounds in Flames - III: The Destruction of DMMP and TMP in a Flame of Hydrogen and Oxygen // Combustion and Flame, Vol. 121, 2000, pp. 593 - 609.
22. Korobeinichev O.P., Ilyin S.B., Mokrushin V.M., and Shmakov A.G. Destruction Chemistry of Dimethyl Methylphosphonate in H<sub>2</sub>/O<sub>2</sub>/Ar Flames Studied by Molecular Beam Mass Spectrometry // Comb. Sc. & Tech., 1996, Vol. 116 - 117, pp. 51 - 67.
23. Korobeinichev O.P., Ilyin S.B., Shvartsberg V.M., and Chernov A.A. The Destruction Chemistry of Organophosphorus Compounds in Flames - I: Quantitative Determination of Final Phosphorus-Containing Species in Hydrogen-Oxygen Flames // Combustion and Flame, Vol. 118, 1999, pp. 718 - 726.
24. Yanenko N. N. The Method of Fractional Steps for Solving Multi-Dimensional Problems of Mathematical Physics in Several Variables. Springer-Verlag, Berlin, 1971.
25. Harlow F. H., and Welsh J. E. Numerical Calculation of Time-Dependent Viscous Incompressible Flow of Fluid with Free Surface // Physics of Fluids, Vol. 8, 1965, pp. 2182 - 2189.
26. Tereshenko A. G., Korobeinichev O. P., Skovorodko P. A., Paletsky A. A., and Volkov E. N. Probe Method for Sampling Solid-Propellant Combustion Products at Temperatures and Pressures Typical of a Rocket Combustion Chamber // Combustion, Explosion, and Shock Waves, Vol. 38, No. 1, 2002, pp. 81 - 91.
27. Skovorodko P. A. Two Approaches to Simulation of the Flow in the Flooded Jet // Mathematical Simulation, Vol. 15, No. 6, 2003, pp. 95 - 100 (in Russian).
28. Broc A., De Benedictis S., Dilecce G., Vigliotti M., Sharafutdinov R. G., and Skovorodko P. A. Experimental and Numerical Investigation of an O<sub>2</sub>/NO Supersonic Free Jet Expansion // J. Fluid Mech., Vol. 500, 2004, pp. 211 - 237.
29. R. J. Kee, F. M. Rupley, and J. A. Miller. Chemkin-II: A Fortran Chemical Kinetics Package for the Analysis of Gas Phase Chemical Kinetics. Sandia National Laboratories Report No. SAND89 - 8009B (1989).
30. Galkin V. S. Slip Effects in Weakly Rarefied Hypersonic Flow around Bodies // Inzh. Zh., Vol. 3, No. 1, 1963, pp. 27 - 36 (in Russian).
31. Hirschfelder J. O., Curtiss Ch. F., and Bird R. B. Molecular Theory of Gases and Liquids. Wiley, New York, 1954.